TECTONOSTRATIGRAPHIC COMPLEXITY AND FAULT DAMAGE ZONES IN THE CAÑON CITY EMBAYMENT, COLORADO

By

ABUBAKAR ENEYE ALIYU

(Under the Direction of Christian Klimczak)

## ABSTRACT

The Cañon City Embayment (CCE), which is situated in the southernmost portion of the Denver Basin in Colorado has been described as an area with complex geology. Newly observed tectonostratigraphic relationships in the area have been documented through detailed lithologic and structural mapping. Two generations of thrust faults and two generations of unconformities are present and are interpreted to be linked to the Ancestral and Laramide orogenies, respectively. Structural measurements and analysis of bedding planes, faults and fault zones, joints, slickensides, deformation bands, and unconformities show that these structures are consistent with the NW-SE orientation like those of the Ancestral and Laramide uplifts. Radiometric age dating in future studies would provide exact ages of the unconformities and thrust faults.

INDEX WORDS: Deformation bands, Ancestral Rocky orogeny, Laramide orogeny

# TECTONOSTRATIGRAPHIC COMPLEXITY AND FAULT DAMAGE ZONES IN THE CAÑON CITY EMBAYMENT, COLORADO

By

ABUBAKAR ENEYE ALIYU

B.S., Ahmadu Bello University, Nigeria, 2011

M.S., Ahmadu Bello University, Nigeria, 2016

A Dissertation Submitted to the Graduate Faculty of The University of Georgia in Partial Fulfillment of the Requirements for the Degree

MASTER OF SCIENCE

ATHENS, GEORGIA

2024

TECTONOSTRATIGRAPHIC COMPLEXITY AND FAULT DAMAGE ZONES IN THE

CAÑON CITY EMBAYMENT, COLORADO

By

ABUBAKAR ENEYE ALIYU

Major Professor: Christian Klimczak

Committee: Douglas Crowe

Kelsey Crane

Electronic Version Approved:

Ron Walcott
Vice Provost for Graduate Education and Dean of the Graduate School
The University of Georgia
December 2024

ACKNOWLEDGEMENTS

First and foremost, I would like to thank my advisor, Dr. Christian Klimczak, for his continuous guidance, encouragement, and invaluable feedback. His expertise and patience have been instrumental in the successful completion of this thesis. I am also deeply grateful to my committee members, Dr. Douglas Crowe and Dr. Kelsey Crane, for their insightful suggestions and constructive criticism. Their input has significantly enhanced the quality of this thesis.

I want to thank my field assistant, Rain Morrison, the UGA 2023 field camp students, Chris Fleisher and other faculties and staff that came out with us to the field.

A special thanks goes to all the graduate students of the department, who provided a stimulating and fun environment in which to learn and grow. Your support and friendship have been invaluable throughout this journey.

I am indebted to my family for their unwavering support and understanding. Their belief in me has been a constant source of motivation.

Finally, I would like to express my gratitude to AAPG and the Department of Geology, through the Allard Geology Award, for their financial support which played a crucial role in making this research possible.

TABLE OF CONTENTS

LIST OF TABLES

LIST OF FIGURES

# CHAPTER ONE

## Introduction

### 1.1 Geological Setting of the Cañon City Embayment

The field area mapped in this project is in the Colorado Front Range, near Cañon City. Unique tectonostratigraphic and juxtaposition relationships of rocks were observed within a specific small location in the Cañon City Embayment (CCE), marked by the yellow pin in the study area map (Fig. 1). The CCE area is positioned between the junction of the Wet Mountains and the Front Range of the Colorado Rocky Mountains (Gerhard, 1967). The author noted that the northern edge of the CCE borders the southernmost parts of the Front Range.

Extensive geological studies have been conducted on the CCE in Colorado. The complex geology there occurs within the Colorado Mineral Belt, as indicated by Flynn and Barber (2000). The tectonic development of the CCE dates to the Paleozoic era (Gerhard, 1967) with the boundaries of the embayment defined by high-angle reverse faults, particularly noticeable in the northern region. The author also noted that the existence of the reverse faults suggests a potential horizontally compressional tectonic cause for the down-dropped regions.

Gong (1986), through mapping of the lithofacies and thicknesses of Pennsylvanian rock formations in Southeastern Colorado, noted that during the onset of the Pennsylvanian, areas now occupied by Cañon City, the Wet Mountains, and the Front Range of the Rockies were part of a low-lying landmass. The Morrowan sea encroached from the Anadarko Basin on the flanks of the landmass but was unable to cover it. Towards the end of the Morrowan sub-period, uplift and faulting occurred in the vicinity of the current Front Range and Wet Mountains, leading to the formation of the Ancestral Rocky Mountains. The Laramide orogeny took place between 80 and 40 million years ago (Coney, 1971), and produced a great deal of basins and uplifts in the foreland of western North America. Syn- and post-orogenic sediments were formed during the Laramide orogeny, resulting in the formation of two foreland basins: the Denver Basin, which houses the Cañon City Embayment, and the Raton Basin (Gong, 1986). The post-Laramide uplift of the northern part of the Rio Grande Rift may be explained by the Colorado Plateau, which is a concentrated dynamic topographic high (Moucha et al 2008). A strong mantle upwelling associated with the sinking Farallon slab is assumed to underlie the Colorado Plateau. So, Proterozoic rifting, the Ancestral Rocky Mountain Orogeny, the Laramide Orogeny, and the uplift of the Colorado Plateau are some of the significant tectonic events that have impacted and shaped the region (Holmes, 1956; Gerhard, 1967; Gong, 1986).

## 1.2 Stratigraphy

Numerous studies have been conducted on the stratigraphy of the CCE (e.g., Frederickson et al., 1956; Webster, 1959; Gerhard, 1967; Gong, 1986). The CCE has traditionally been described to be made up of Precambrian crystalline basement rocks and sequences of sedimentary rocks of Ordovician to Cenozoic ages. These rocks include the following: Proterozoic Basement Rocks, Lower Ordovician Manitou Formation, Middle Ordovician Harding Formation, Upper Ordovician Fremont Formation, Pennsylvanian Fountain Formation, Middle Jurassic Ralston Creek Formation, Upper Jurassic Morrison Formation, Dakota Group and Benton Group (Fig. 2).

Granitic intrusives with a sequence of metamorphosed sediments make up the Pre-Cambrian rocks (Frederickson et al., 1956). The Ordovician Manitou Formation outcrops almost continuously in a narrow strip throughout the embayment (Gong, 1986), and rests noncomformably on the Precambrian basement. Gong (1986) described the angle of contact between the underlying crystalline rocks and the Manitou Dolomite to be high. The Middle Ordovician Harding Formation is next on the stratigraphic column and it is made up of red, white, and green quartz arenite sandstones that are fine to coarsely grained, well-rounded, moderately sorted, porous, and interbedded with subsets of sandstone and variegated shale (e.g., Anlian, 2017). The Harding Sandstone is overlain by the Fremont Formation, which is indicated by a yellow weathered zone (Webster, 1959). Together with the Manitou Formation, the Fremont Formation is a cliff-former that mainly emerges in the northern part of the CCE. It is found to overlay conformably the Harding Formation. The Pennsylvanian Fountain formation is a composed of interbedded sandstone, shale, siltstone, and coarse arkosic conglomerate in the embayment area (Frederickson et al., 1956). It was reported therein that the unit thickness varies from around 4,500 feet at Colorado Springs to 1,000 feet east of Cañon City. The sediments that make up the Fountain are derived from the Ancient Rocky Mountains, constituting syntectonic and post-orogenic deposits in this sequence (Gerhard, 1967). Above the Fountain is the Middle Jurassic Ralston Creek Formation. It crops out continuously from west to east in the embayment (Gong, 1986). The thickness of this formation in the embayment ranges from 27 feet to 170 feet (Frederickson et al., 1956). Above the Ralston Creek, the Upper Jurassic Morrison Formation is exposed along hogback and escarpment slopes in the CCE (Gong, 1986). It overlies conformably the Ralston Creek Formation. The Dakota group succeeds the Morrison Formation in the stratigraphic column. The Dakota group is made up of three members which are the Lower Cretaceous Lytle Sandstone, Lower Cretaceous Glencaire shale, and Lower Creatceous Dakota Sandstone. These members are found to be locally offset by faulting (Gong, 1986). The Dakota group is overlain by the Benton group. The Benton group can be divided into three members, specifically the Graneros shales, Greenhorn limestone, and Carlile shale (Gong, 1986). Relationships between all these sedimentary formations have been reported by these authors to be either nonconformable or disconformable (Fig. 2).

### 1.3 Tectonic Events (orogenesis) of the area

Brown (1978) through seismic reflection data obtained from the Cañon City-Pueblo area, indicates the occurrence of two distinct phases of tectonic activity: the initial phase of tectonic activity, the Ancestral Rocky Mountain orogeny, from the early Pennsylvanian to the mid-Pennsylvanian period and the subsequent Laramide orogeny, attributed to the Late Cretaceous.

#### 1.3a. Ancestral Rocky Mountains Orogeny

During the Pennsylvanian–Permian period, the Ancestral Rocky Mountains emerged as a collection of intracratonic block uplifts or highlands primarily involving the basement rock in Colorado and neighboring areas (e.g., Kluth & Coney, 1981; Hoy & Ridgway, 2002). These sequences of basement highs are associated with intervening sedimentary basins of considerable structural depth (e.g., Hoy & Ridgway, 2002; Sweet & Soreghan, 2010).

It started with suturing in the early Pennsylvanian in the Ouachita region and by the middle Pennsylvanian period, the extent of this suture zone expanded and became active from the Ouachita to the Marathon region. Gradually, the scale of this cratonic deformation intensified and expanded geographically, which led to the formation of the Ancestral Rocky Mountains

(Kluth & Coney, 1981). Gerhard (1967) suggested that the Ancestral Rocky Mountains emerged in the vicinity of the Laramide ranges in central Colorado either towards the end of the Mississippian or the start of the Pennsylvanian period.

The Ancestral Rockies are made up of extensive block uplifts that are bounded by narrow fault zones (Fig. 3). They are primarily oriented northwest, with intervening sedimentary basins (Haun & Kent, 1965; Sweet & Soreghan, 2010). Evidence for these uplifts is deduced from unconformities and deposition of coarse, arkosic sediments eroded from them (Kluth & Coney, 1981). They exhibit structural relief of up to 5 kilometers (Barbeau, 2003). The most substantial uplifts were created in present-day Utah, Colorado, and New Mexico (Hoy & Ridgway, 2002).

Despite how significant the Ancestral Rocky Mountain uplifts are and their structural prominence, their tectonic evolution remains ambiguous. Some of the reasons for this could be due to the intraplate location of the ancestral Rocky Mountains, the deformation up to 1500 km from any coeval plate margin, or because of the prolonged history of tectonic activity that has influenced the U.S. Cordillera since the Middle Paleozoic era (e.g., Kluth & Coney, 1981; Kluth, 1998; Burchfiel et al., 1992; Barbeau, 2003). Subsequent Mesozoic and Cenozoic structural overprinting have made identification and interpretation of Ancestral Rocky Mountains structures even more difficult (e.g., Sweet & Soreghan, 2010; Soreghan et al., 2012; Chapin et al., 2014).

Researchers have observed that both the uplifts of the Pennsylvanian-Permian Ancestral Rocky Mountains and those of the Late Cretaceous-Eocene Laramide period (Fig. 4) were outcomes of deformation involving the basement rocks, occurring in the same general region of western North America (e.g., Gerhard, 1967; Hoy & Ridgway, 2002). In contrast to the Laramide uplifts, the mechanisms responsible for the uplift of the Ancestral Rocky Mountains are not well understood, primarily due to the limited identification of structures definitively associated with the late Paleozoic era. Many of the structures are thought to have been reactivated during Late Cretaceous–Eocene Laramide shortening and/or during Cenozoic extension. Therefore, the effects of Laramide deformation and subsequent erosion have largely obscured most structural features predating the Laramide era. (e.g., DeVoto, 1980; Tweto, 1980; Weimer, 1980; Lindsey et al., 1983; Hoy & Ridgway, 2002).

Sweet & Soreghan (2010) mention that the geometry and slip of faults are frequently poorly constrained, mostly because of overprinting by younger deformational processes and inaccurate dating of basin fill. So, a lack of exact age data as well as geometric and kinematic constraints from individual faults has hampered their ability to understand the tectonic evolution of the ancestral Rocky Mountains. Gerhard (1967) suggests that theories of recurring or resurgent tectonics may be applied to this region, according to the interpretation of the correspondence between the structural features of the Laramide orogeny and those of the Ancestral Rocky Mountains.

The formation of the Ancestral Rocky Mountains was connected to the convergence of North America with South America-Africa. Kluth & Coney (1981) noted that the deformation of North America during the Pennsylvanian period shares some similarities with the intraplate deformation of Asia, in the Cenozoic era, which was in response to the collision with India. Many contradictory hypotheses have been proposed to explain the formation and uplift of the Ancestral Rocky Mountains. These include normal, reverse, and thrust faulting, strike-slip faulting, and near-vertical faulting (DeVoto, 1980; Kluth and Coney, 1981a, 1981b, 1983; Goldstein, 1981; Warner, 1983; Budnick, 1986; Kluth, 1986; Lindsey et al., 1986a). Plate tectonic settings suggested to have formed the Ancestral Rocky Mountains include continent-to-continent collision along the southern margin of North Ameria (Kluth and Coney, 1981; Kluth, 1986; Dickinson and Lawton, 2003) or by Andian-type subduction along Laurentia's southwestern margin (Ye et al., 1996).

Important insights on the types of deformation that led to the uplift of the mountain range can be obtained from syn-orogenic strata e.g., Lawton, 1985; DeCelles et al., 1987; Burbank and Vergés, 1994; Lawton et al., 1999). Synorogenic strata are frequently deformed in unison with uplift. So, the tectonic development of these structures can be inferred from faults and folds that formed in synorogenic strata next to Laramide basement uplifts (e.g., DeCelles et al., 1991; Hoy and Ridgway, 1997).

(Gerhard, 1967) gained insights into the early Paleozoic history from variations in thickness and lithology among early Paleozoic rock units. He observed that several structural features predating the Pennsylvanian era are retained beneath Pennsylvanian detrital sediments, especially in the CCE, which provides a clear example of the extensive erosional and angular pre-Pennsylvanian unconformity that characterizes the Ancestral Rocky Mountain orogeny.

More recently, the timing and style of individual faults of the ancestral Rocky Mountains have been distinguished from younger deformational events within the Central Colorado trough (Hoy and Ridgway, 2002) and the Paradox basin (Barbeau, 2003; Thomas, 2007; Moore et al., 2008) using structural relationships, modeling, synorogenic strata, and intraformational unconformities. To date, there is insufficient proof to back up a single structural theory explaining how the uplifts of the Ancestral Rocky Mountains developed (Kluth, 1998).

### 1.3b. Laramide Orogeny

Block uplifts in the Rocky Mountain fold and thrust belt in the United States, Canada, and Mexico (Fig. 4) were caused by late Cretaceous to Paleocene (80 to 55 Ma) orogenic processes like the Laramide Orogeny (e.g., Bird, 1998; English and Johnston, 2004; Copeland et al., 2017). Synorogenic sediments found on the sides of the Wet Mountains and Front Range show that Laramide uplift of these features began in the Late Cretaceous (Tweto 1975; Kluth and Nelson 1988). Laramide orogenic deformation resulted in the formation of a network of so-called basement-cored arches, which delineated the northern and eastern edges of the Colorado Plateau and shaped the elliptical sedimentary basins within the Rocky Mountains (Erslev et al., 2004). The most distinctive features from this period are the basement-cored uplifts (Blakey et al., 2018). The Laramide event was initially identified by sedimentary deposits in the Laramie Basin of southern Wyoming (Blakey et al., 2018). The authors stated therein that the basins underwent downward faulting, receiving eroded material from the uplifted areas. It was also noted that it was the basin deposits rather than the uplifts that provided geologists with clues about the Laramide orogeny. Laramide formations resemble the Ancestral Rocky Mountains uplift in terms of size and design (Barbeau, 2003).

The Laramide orogeny contributed to the creation of the Rocky Mountains and posed a problem that plate tectonics theory is unable to satisfactorily address (e.g., Brewer et al., 1980; Maxson and Tikoff, 1996; Copeland et al., 2017; Carrapa et al., 2019). There are ongoing debates over the tectonic mechanism underlying Laramide deformation. Some theories include subcrustal shear during low-angle subduction (Bird 1988, 1998; Hamilton 1988) and upper crust detachment during plate coupling to the west (Lowell 1983; Oldow et al. 1989; Erslev 1993). The following methods have been proposed to explain the orogenesis of Laramide: flat-slab subduction, retroarc thrusting, "orogenic float" tectonics, and Cordilleran transpressional collision. The Laramide orogeny is thought to have occurred after the terranes that comprise the majority of the North American Cordillera accreted during the Jurassic and late Early Cretaceous (Dickinson and Snyder, 1978; Monger et al., 1982; Monger and Nokleberg, 1996; Dickinson and Lawton, 2001). As a result, a collisional origin for Laramide orogenesis has been ruled out.

The most popular theory to explain Laramide orogenesis in the United States is flat-slab subduction, in which stresses are transmitted eastward by the stress coupling of a subhorizontal oceanic slab to the upper plate, resulting in basement-cored block uplifts and arc magmatism in the foreland. According to a series of studies (e.g., Ye et al., 1996; Liu and Currie, 2016; Blakey et al., 2018; Erslev et al., 2022), it was the flat-slab subduction (Fig. 4) of the Farallon plate and the oceanic plateau that rides on it that led to the Laramide orogeny and Laramide deformation in the Rocky Mountain region. Liu and Currie (2016) suggested that the Laramide orogeny took place more than 1000 km of the Farallon subduction plate boundary. According to Maxson and Tikoff (1996), the Laramide orogeny was a collisional orogeny like the modern Himalayan and prehistoric Hercynian orogenies. As an alternative to the shallow slab model, they proposed a hit-and-run collision model.

The explanations for the diversity of Laramide structural trends, which include faults, folds, and arches trending in almost every direction, include the reactivation of pre-existing weaknesses in the basement (Hansen 1986; Stone 1986; Blackstone 1990; Chase et al. 1993) and multiple stages of differential oriented compression (Chapin and Cather 1981; Gries 1983; Bergh and Snoke 1992).

## 1.4 Motivation

A field locality in the CCE exposes newly recognized tectonostratigraphic relationships, where the individual rock units are juxtaposed to one another by a series of unconformities and faults. These relationships are recorded from a previous University of Georgia M.S. thesis (Anlian, 2017) and continued observations by Dr. Christian Klimczak (advisor of this thesis research) and Dr. Dave Barbeau (University of South Carolina, personal communication). We hypothesize that two generations of thrust faults produced two types of deformation within the Ordovician Harding Formation, i.e., a tectonic quartzite confined to narrow zones surrounding the first generation of thrusts and deformation bands that surround the second generation of thrusts.

In this project, I have documented, through field mapping and structural measurements, this newly observed tectonostratigraphy in the CCE and have also characterized the two major thrust faults and their damage zones.

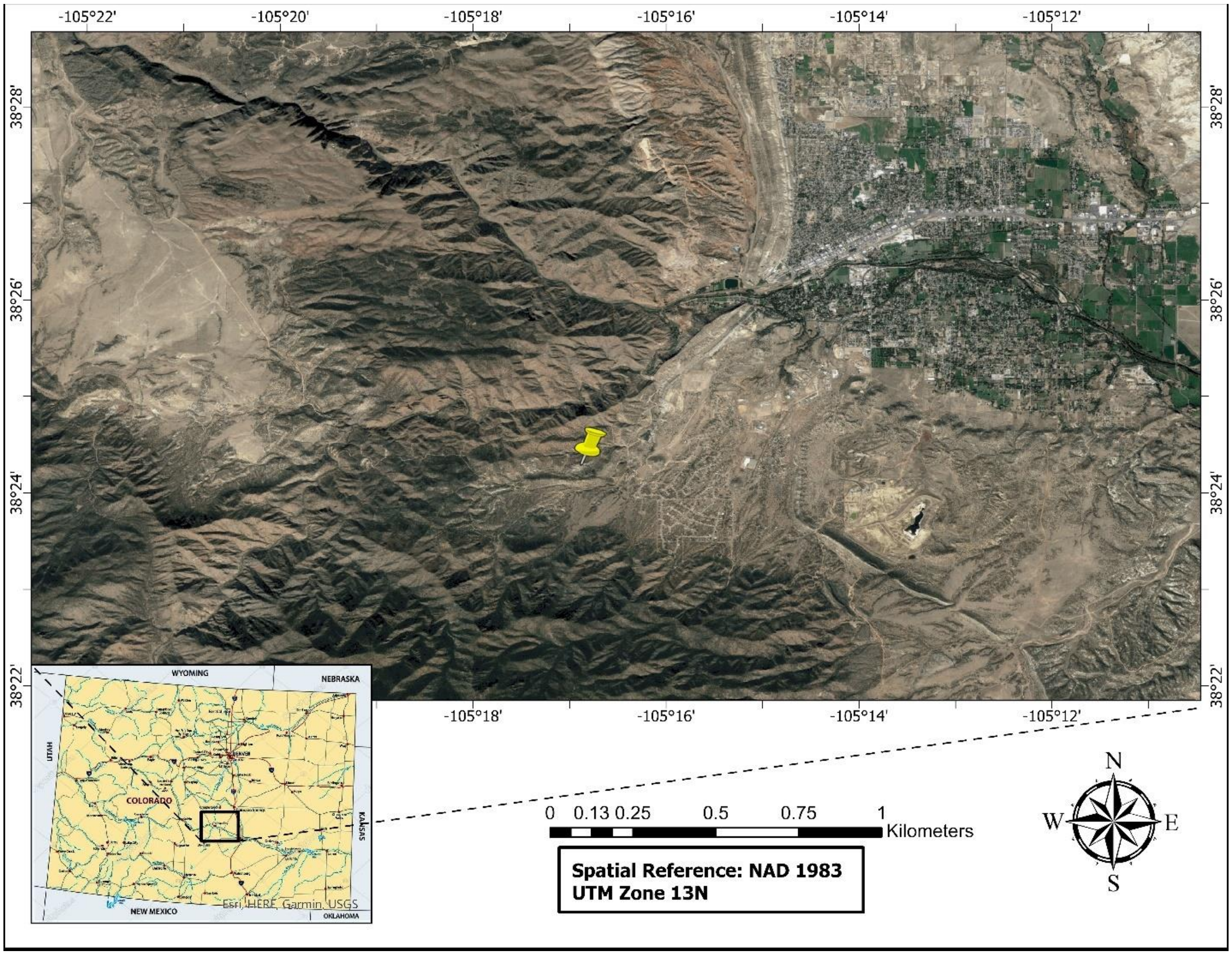


**Figure 1**. Location map of the study area where geological mapping was carried out within the Cañon City Embayment.

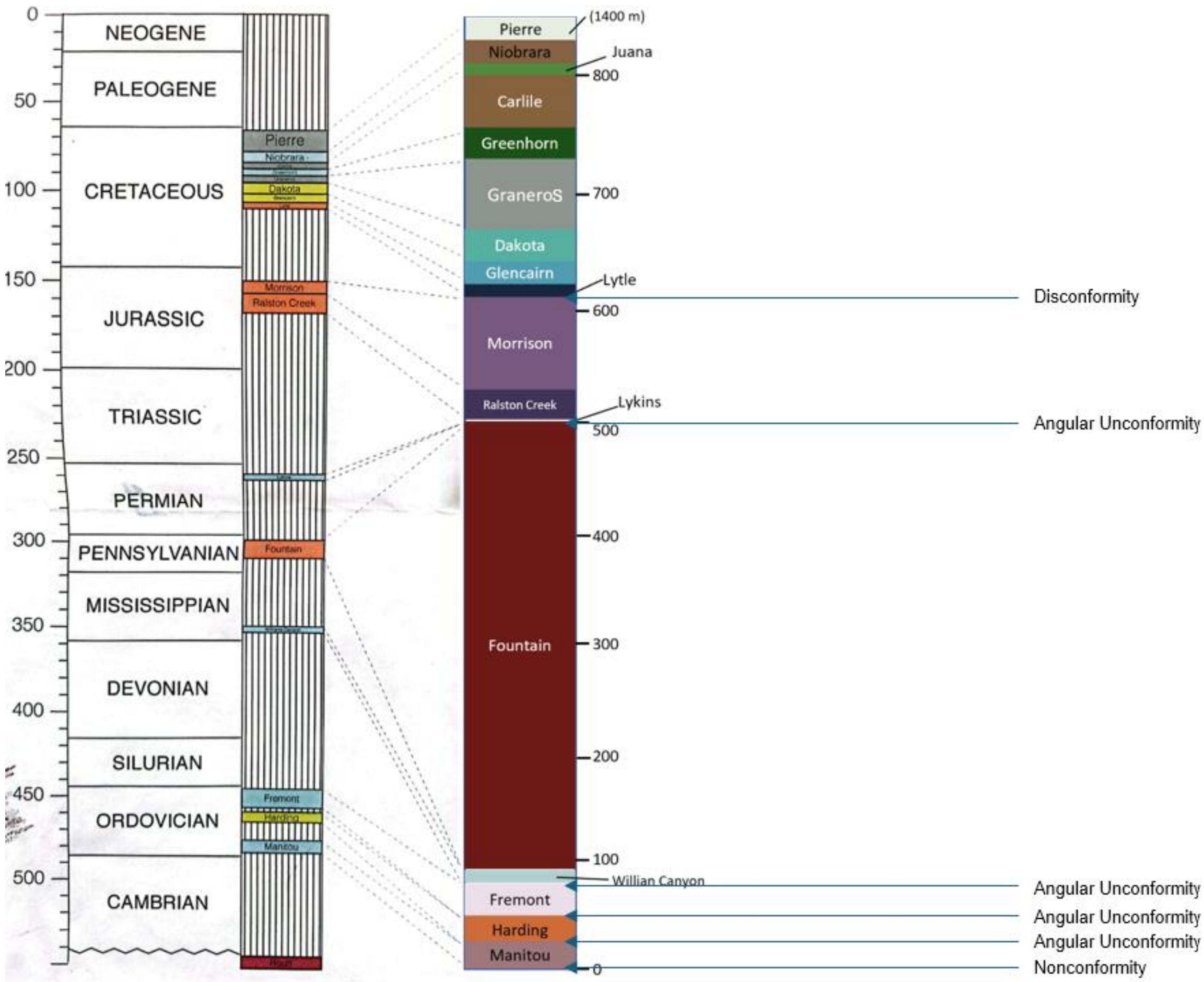


**Figure 2.** Stratigraphy of the Cañon City Embayment.

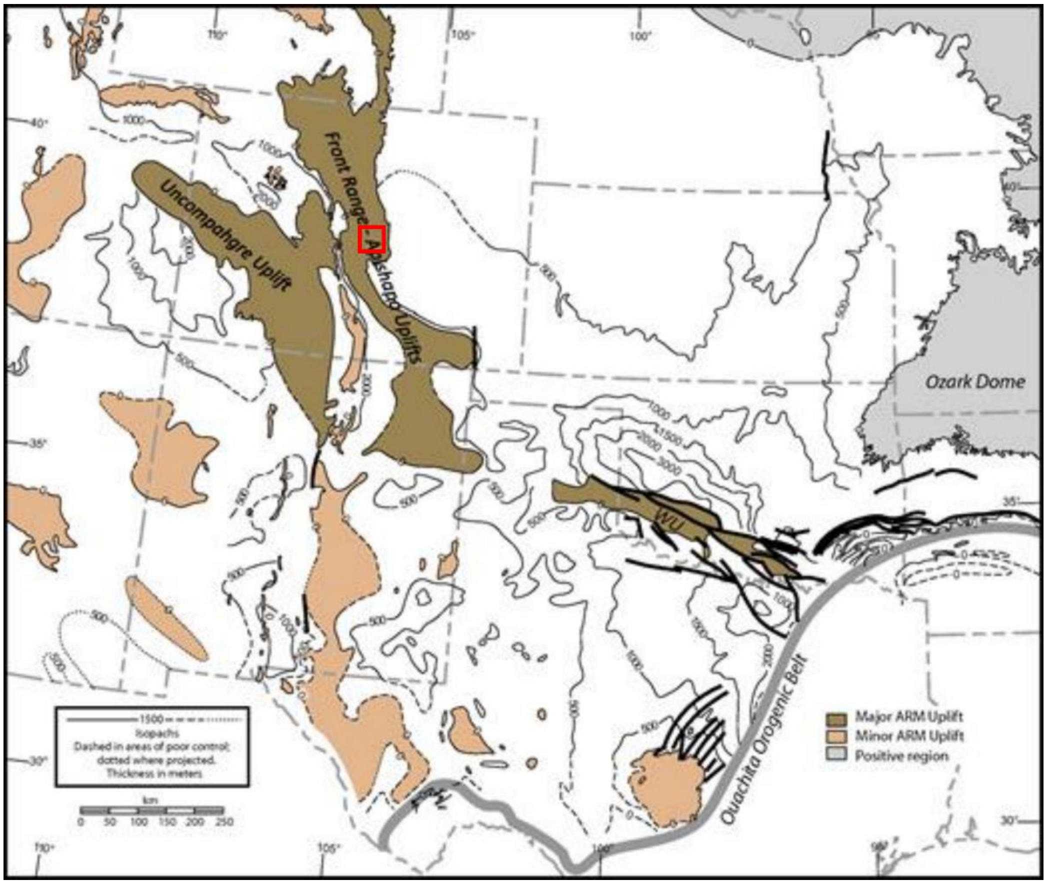


**Figure 3.** Sedimentary basins of the Ancestral Rocky Mountains and Late Paleozoic Precambrian basement-cored uplifts. The figure is taken from Soreghan et al. (2012) and Sweet et al. (2021). Bold black lines represent faults. The CCE within this region is represented by the red box.

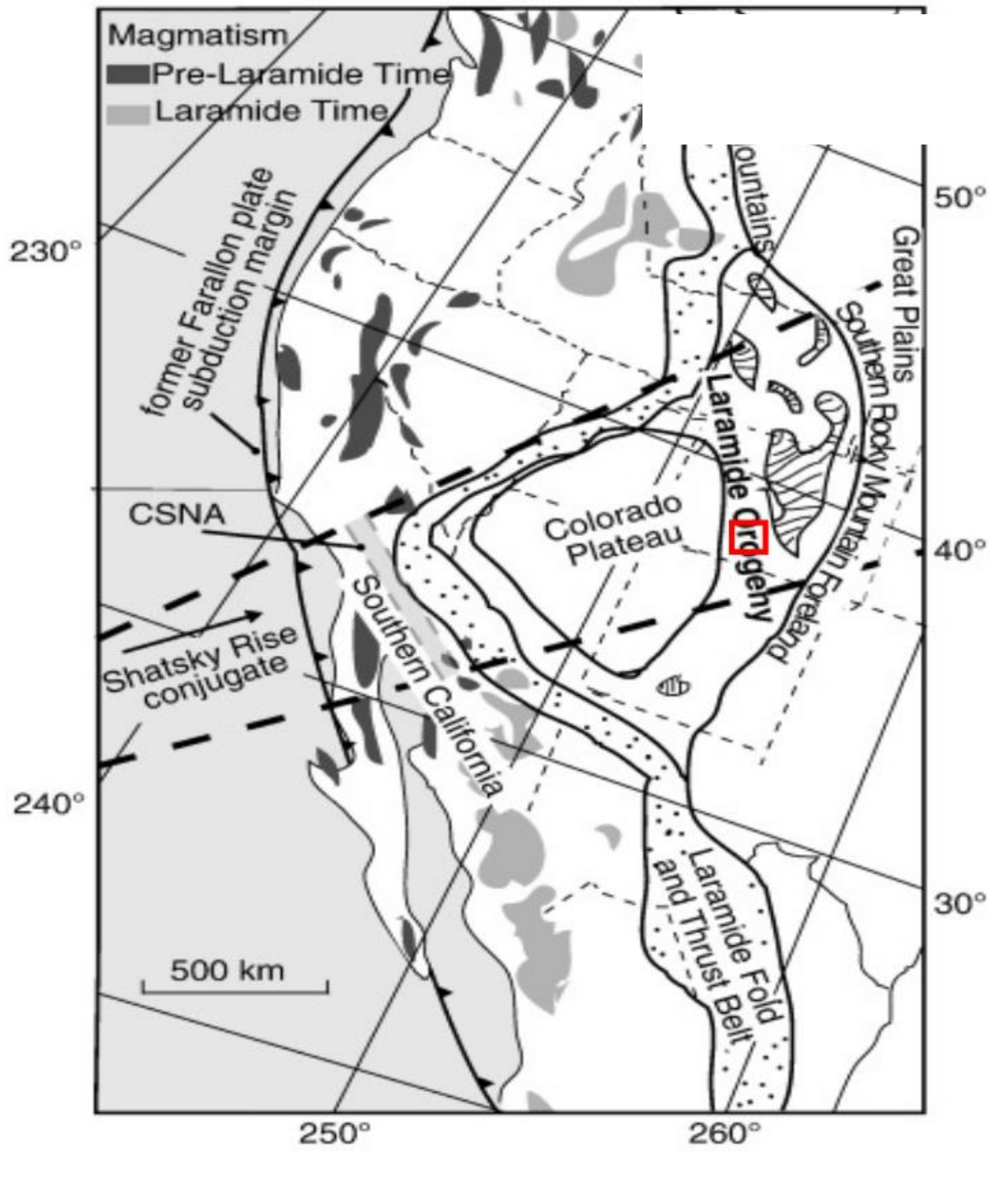


**Figure 4.** A map displaying the tectonic characteristics of the Farallon plate subduction (after English and Johnston, 2004). The CCE is represented by the red box.

# CHAPTER TWO

## Methods

This project focuses on geologic data collection in the CCE through lithological mapping of the various rock units and detailed structural mapping of planar structures like bedding, faults, and unconformities. Mapping was carried out together with a UGA undergraduate field assistant for about 35 days. The data collected was used to produce a series of structural and geological maps, carry out structural analysis to understand the original stratigraphy and orientation of the beds before deformation, and permeability analysis to understand the difference in permeability between the different kinds of fault damage zones. Micro-structural analysis was also carried out on samples collected within the fault damage zones to evaluate deformation at the microscopic scale.

Lithological mapping was carried out by focusing on one exposure at a time. For exposures with different rock types, I divided the exposure into units based on features like changes in color, texture, and mineralogy. I observed the nature of the contacts between rock units (whether they are sharp or gradational), and whether they are depositional or unconformity contacts.

I examined evidence of displacement and deposition, conducting detailed inspections of each rock unit to identify their distinguishing characteristics. I sketched each exposure, recorded my observations in my field notebook, and collected representative samples as needed. To understand the area's tectonostratigraphy and determine the initial orientation of the beds prior to the unconformities, I visited all locations with evidence of unconformities. There, I measured the orientations of the beds above and below the unconformities, as well as the orientations of the unconformities themselves. I determined the presence of these unconformities where I see evidence of gap in the depositional history of the rock units. These are locations where we have missing records of rocks, thereby creating an unusual contact between rocks of very different ages.

Bedding orientations measurements of the individual rock types, orientation of faults, unconformities and deformation bands were collected using both a Brunton compass and the FieldMove Clino app, a free geology app for Android handheld devices, by Petroleum Experts Limited. This application allowed me to use my Android device as a digital compass-clinometer, capturing field data using its built-in GPS. To carry out these measurements successfully, we went around the field area and stopped to take strike and dip measurements directly on outcrops wherever we saw depositional contacts and unconformity related contacts. For faults, we measured the strike and dip of the fault planes and, where present, the trend and plunge of the slikenlines associated with the slickenside surfaces of the faults. Slickensides and slickenlines give us clues regarding the direction and sense of motion on a fault. Deformation bands measurements were taken directly from the outcrop surfaces by orienting my android phone with the Clino app opened, parallel to each deformation band. Where planar surfaces are uneven, I used a notebook or clipboard to smooth out the unevenness. All recorded measurements were stored automatically in the FieldMove app and photographs of the associated contact surfaces and structures were taken were taken at the exact locations. This FieldMove Clino data was exported to my field computer as move file (.mve), Google Earth file (.kmz) and as CSV files. These field data were processed in the lab using ArcGIS pro, Stereonets, and the MOVE structural geology modeling software by Petroleum Experts.

I found all exposures of Ordovician Harding sandstone in the map area and determined whether they are undeformed, crystallized, or contain deformation bands (e.g., Fossen and Bale, 2007; Fossen et al., 2018). I also documented the nature of the two different fault damage zone types present by classifying and comparing them to one another in terms of rock properties like porosity, permeability, and deformation mechanisms. After completing the lithological and structural mapping of the area, I carried out a systematic mapping to determine permeability reduction within porous Harding Sandstone caused by the presence of deformation bands. I took permeability measurements along the surfaces of both the deformation band Harding Sandstones and the host sandstones with a portable TinyPerm II instrument along a Scanline. The TinyPerm II is an air permeameter which can determine the permeability of rock matrix from the surface of the rock. It is developed by a company known as New England Research, Inc. This company specializes in measuring and interpreting rock properties specifically for the energy sector. The Scanline is a rope with marked off meter increments which was laid down along the surface of the rocks where permeability measurements were collected.

Along the scanline, ten measurements at approximately every ten centimeters were collected for every one meter along the scanline. Permeability measurements are displayed as response function (T) on the screen of the microprocessor and control unit of the TinyPerm. I took 51 measurements for deformation bands Harding Sandstone, 31 measurements for silicified Harding and 41 for undeformed Harding. These readings were recorded in my field notebook. All measurements collected were imported into Microsoft excel, and the response functions (T) were converted to permeability measurements in millidarcy (mD) using the equation: $T = -0.8206 * \log_{10}(K) + 12.8737$ (NER, Inc.).

Samples of the two different fault rocks were collected from the fault zones present in the field site for microstructural analysis. Structural diagenesis (e.g., Laubach, 2010; Rodrigues et al., 2021) and deformation mechanisms of fault rocks were analyzed in the laboratory from rock samples at microscopic scale through thin section analysis. This analysis was done using the Nikon petrographic microscope and photomicrographs were taken with the aid of a camera and computer attached to this microscope. The different micro deformation mechanisms, such as different types of grain boundary migrations or cataclasis gave an insight into the strain rate and temperatures involved in the deformation.

# CHAPTER THREE

## Description of Stratigraphic Units

### 3.1 Proterozoic Basement

The Proterozoic Basement exposures mapped in the study area, referred to as Mixing Bowl by UGA faculty, are all made up of gneiss. They are mainly found in the northern portion of the study area extending laterally from east to west and in the central part of the study area (Fig. 5). Different varieties of gneiss are found here, and they include a pinkish, brown to reddish crystalline rock formed by enormous amounts of orthoclase feldspars and biotite minerals, and a bright-grayish gneiss which is made up of quartz, plagioclase feldspars, and biotite. The basement is mostly composed of mineral crystals which are medium grain in size. They are massive where found un-weathered or undeformed, and occur as sheared, friable materials in areas where they exist in association with or very close to faults and fractures. Structures such as joints, minor faults, foliations are pervasive in some of the basement gneiss exposures (Fig. 6).

### 3.2 Manitou Formation

The Lower Ordovician Manitou Formation is only exposed in one location within the Mixing Bowl as a very thin (about 12 cm thick) sliver of heavily sheared rock. This is at the southern portion of the map, very close to the Ralston Creek Formation. It is found existing in fault contact with thick, massive exposure of white deformation banded Harding sandstone and a highly weathered and friable, sheared pinkish gneiss (Fig. 7). The Manitou ranges in color from dark gray to dark purple, occurring as splinters of rock fragments. Collecting consolidated, compact samples of Manitou was almost impossible without shattering it.

### 3.3 Harding Formation

The Middle Ordovician Harding Formation is made up of whitish, pinkish to reddish-brown, almost horizontal layers of quartz arenite sandstone and variegated shale beds (Figs. 8, 9), and often found in the study area in fault contact with Basement rocks, especially in the northwestern and central areas. In some areas in the Mixing Bowl, Harding Sandstone form small, massive exposures of outcrops while others are flat and low-lying. Most of the low-lying Harding are found within stream channels. They lie nonconformably and in contact with the Manitou. The top of the Formation is marked by yellow sandstone beds while the unit at the base is white and is typically a small-pebble conglomerate (Fig. 9). The undeformed Harding occurs as extensive whitish, flat-lying exposures or large outcrops of pink to brown beds of sandstones and shales (Fig. 9). Some undeformed Harding are pinkish red, with alternate purple and yellow banding. They do not possess deformation bands.

#### 3.3a. Deformed Harding Formation

Three types of Harding Sandstones were generally observed. These include the undeformed Harding; the deformation band Harding and the silicified Harding (fig. 10). The Quartzites are associated with the first generation thrust faults while the Deformation Band Harding sandstone units are associated with the second generation thrust faults. This order of deformation is determined from the cross-cutting relationship between the two generations of thrust faults where the second generation thrust fault crosscuts the first one. The major difference between the Harding types is in their color, texture and the presence or absence of a planar structure known as deformation bands. Deformed rocks in the embayment are largely made up of brecciated fault rocks and deformed Harding Sandstones.

The deformation band Harding Sandstone (fig. 11) is white or gray, fine to medium grained and almost recrystallized and is associated with a faulting. It usually contains planar structures of various lengths and thicknesses known as deformation bands (Fig. 11). Deformation bands are very fine-grained, whitish discontinuous bands hosted in porous sandstones. In the embayment, deformation bands were not only restricted to the Harding Sandstone alone, but they were also observed in Fountain Formation, Ralston Creek Formation and Dakota Sandstone. The deformation band Harding is observed mainly in the northern part of the study area, cropping out in an east-west direction. This Harding Sandstone is associated with a thrust fault which is also oriented in an east-west direction. It can be inferred that the deformation band Harding Sandstone was deformed by this thrust fault. There is an observed fault-contact between this Harding unit and the basement.

The silicified Harding is usually light brownish in color and has a crystalline to microcrystalline texture. In the study area, silicified Harding is observed to be oriented in a north-south direction, with exposures in the northern, central, and southern parts. The quarzitified Harding has undergone local deformation and metamorphism, to the extent that they have become quartzites. This deformation of the Harding was caused by thrust faulting. The fault zone within the Harding Sandstone contains rocks surfaces with slickensides and slickenlines (Fig. 12). There is hardly any huge outcrop exposure of this unit in the Mixing Bowl. They usually occur as broken chunks of rocks that have been highly brecciated (Fig. 13).

Structural deformation was observed under the microscope on the scale of individual grains in the quartzite samples (Fig. 14, 15 & 16). These microphotographs of the silicified Harding show evidence of grain boundary migration. In particular, grain boundaries are observed to have bulged into crystals with high dislocation density to form new crystals (Passchier & Trouw, 2005). All the small crystals around it show how the individual crystals form from the big crystal. These observations are indicative of a high strain, low temperature condition, consistent with fault rock and faulting in the upper lithosphere. Some of the quartz contains fluid inclusions in them. These could most likely be primary inclusions.

### 3.4 Fremont Formation

The Upper Ordovician Fremont Formation occurs within the Mixing Bowl as massive mounds of irregularly shaped, dark gray outcrops of dolomite (Fig. 17). It possesses some sugary texture when broken which could be because of a certain degree of metamorphism. These outcrops are usually not very extensive. They are mostly found in depositional contacts with the Harding Sandstone, especially the undeformed Harding in the central and northwestern parts of the study area. Fremont in the Mixing Bowl hardly depicts any layered bedding surfaces. They have very rough and uneven surfaces.

### 3.5 Fountain Formation

The Pennsylvanian Fountain Formation is dark pink to maroon in color. It forms very coarse-grained outcrops of sandstone and conglomerate at its base that are gravel size or bigger, hence it could be described as poorly sorted (Fig. 18). They possess relatively steeply inclined or high angle dipping beds. Fountain exposures form alternate light and dark layers of beds. In most places where exposures of this Formation are found in the study area, they occur as thick beds or layers of sandstone, while in other places, their presence could only be inferred from scattered pieces of conglomerate in very reddish/maroon soil.

### 3.6 Ralston Creek Formation

The Jurassic Ralston Creek Formation ranges in color from white to light gray to light green to brown. It is mostly made up of coarse-grained, weakly cemented and poorly sorted weathered sandstone (Fig. 19). In many places within the study area, it is observed to have deformation bands and interbedded brownish conglomerate clasts. The pebble at its base signifies the top of the Fountain Formation. Just like the Fountain Formation, it has somewhat high angle dipping beds. Ralston Creek exposures in some places within the Mixing Bowl are weathered and broken into chunks (Fig. 20). The outcrop surfaces of this formation are usually highly jointed. There is an unconformity contact between Ralston Creek and the Fountain Formation.

### 3.7 Morrison Formation

The Upper Jurassic Morrison Formation is light brown, fine-to medium-grain sandstone with whitish or light greenish shale layers. In many places within the Mixing Bowl where exposures of the Morrison Formation are found, the shale is as green as the surrounding vegetation (Fig. 21). In many other locations within the study area, the Morrison Formation is observed to be extremely weathered with no distinctive outline. The presence of Morrison Formation was only confirmed from changes in soil coloration due to the weathering of shale. So, the remains of very light green, shaly materials and soil indicate its presence (Fig. 22). Stratigraphically, the Morrison overlies the Ralston Creek Formation, and a depositional contact is generally observed between the two formations.

## 3.8 Dakota Sandstone

The Lower Cretaceous Dakota Formation is a brick-red, white, gray, highly compact, fine-to medium-grained sandstone. It has moderate to high angle dipping beds, and almost vertical in some places resulting in very high and steep cliffs (Fig. 23). These beds are mostly uniformly stacked upon one another. In many locations within the study area, the Dakota sandstone contains deformation bands. These deformation bands found in the Dakota sandstone did not lead to the formation of faults as opposed to what is observed in the Harding sandstone. These deformation bands might just be due to the reduced porosity and permeability in the Dakota sandstones.Within the Mixing Bowl, in areas where the Dakota sandstone is not exposed as high hills and outcrops, it is found as broken chunks of rocks scattered all over. In some locations, Dakota beds dip in opposite directions. At a specific location with coordinate 475482 E, 4250687 N, these opposite dipping Dakota bed signify the presence of a fold with each bed representing a limb. One limb dip to the Southeast and the other dips to the West. The Southeast dipping limb has an orientation of about 27°/007°, while the Southwest dipping limb is 33°/249°. The orientation of the fold axis is 10°/020°.

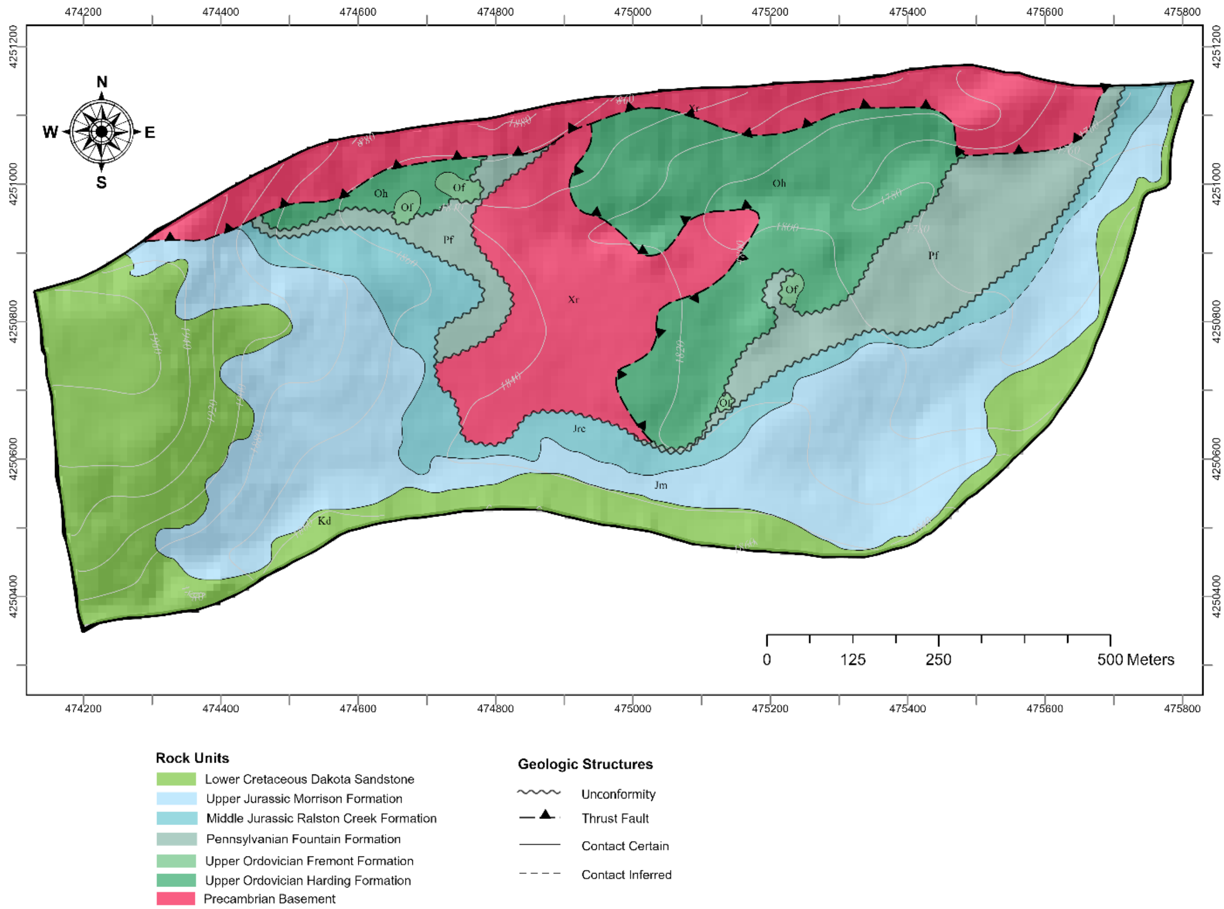


**Figure 5.** Geological map of the study area showing the distribution of all rock units.

**Figure 6.** Outcrop of jointed gneiss, which is the main component of the Proterozoic Basement.

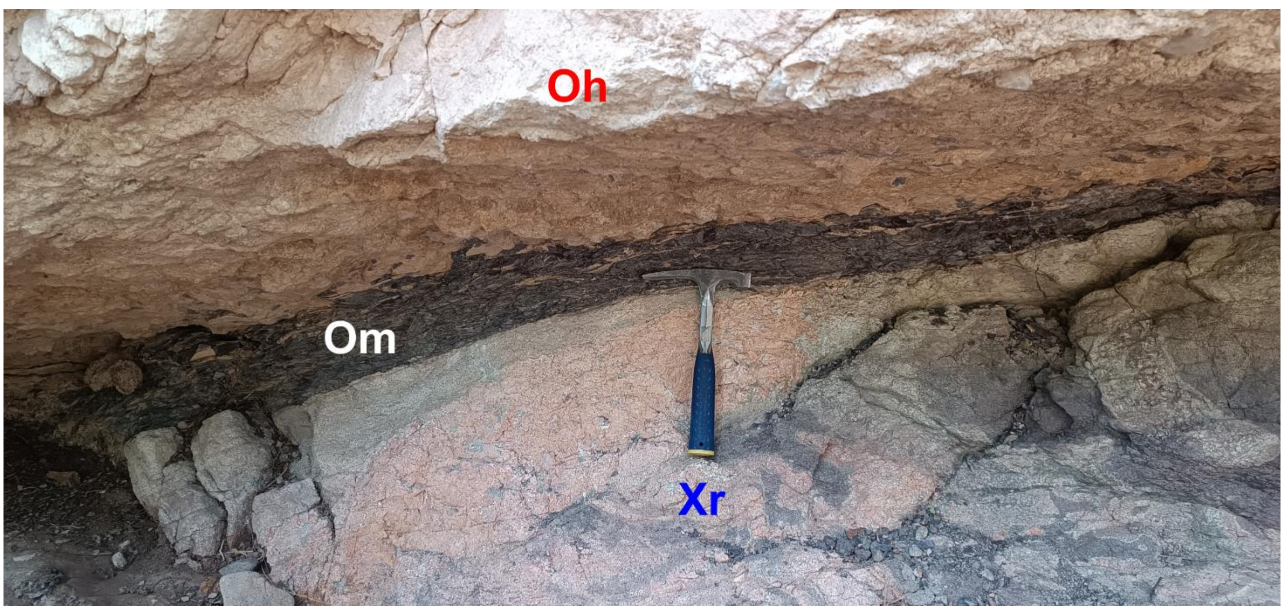


**Figure 7.** Sheared Manitou Formation (middle) in fault contact with Harding Sandstone (top) and sheared gneiss (bottom).

**Figure 8.** Closeup view of the underformed Harding Sandstone.

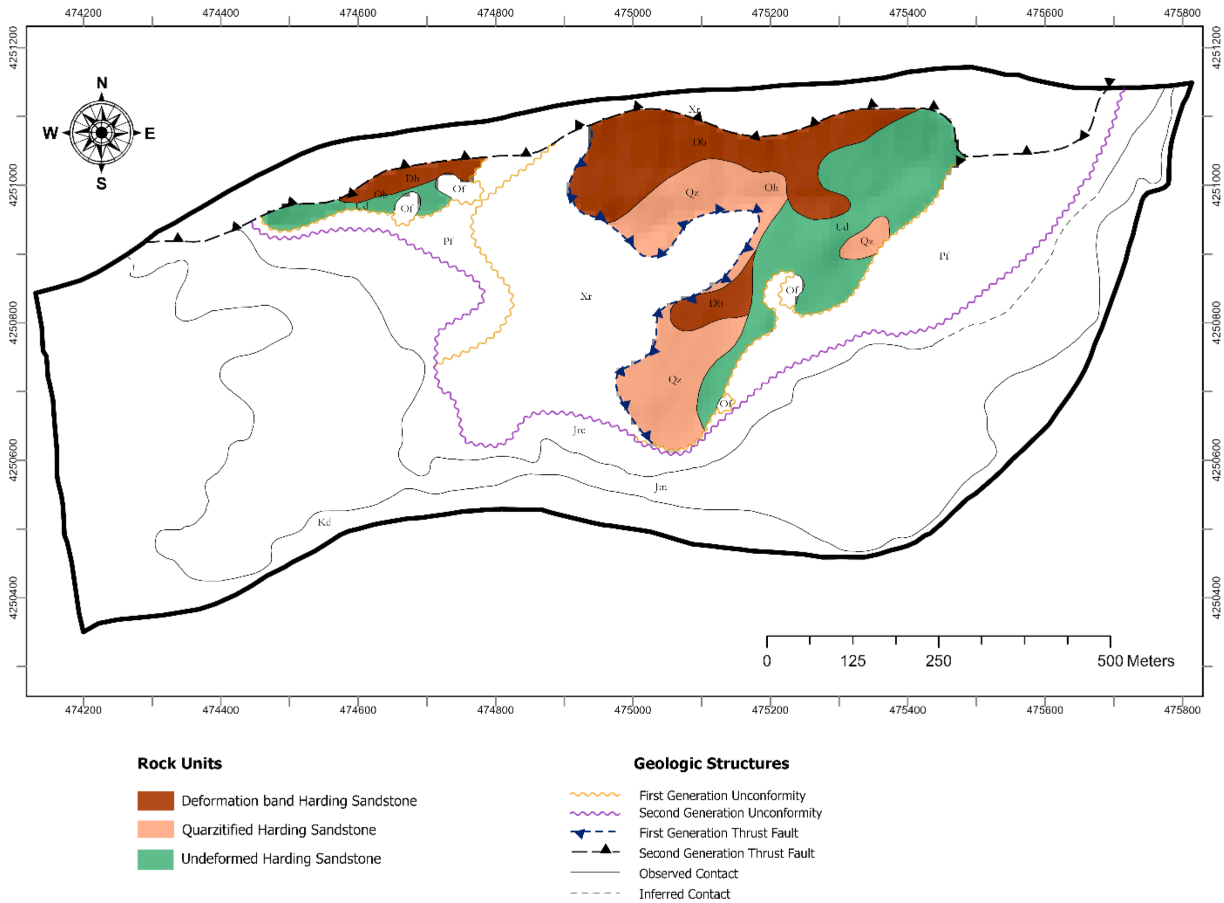


**Figure 9.** Geological map of the different varieties of Harding Sandstone in the study area.

**Figure 10.** Deformation Band Harding Sandstone outcrop. The whitish vein-like features on its surface are deformation bands.

**Figure 11.** Tectonically silicified Harding revealing slickensides of a fault plane.

**Figure 12.** Brecciated, silicified Harding within fault damage zone.

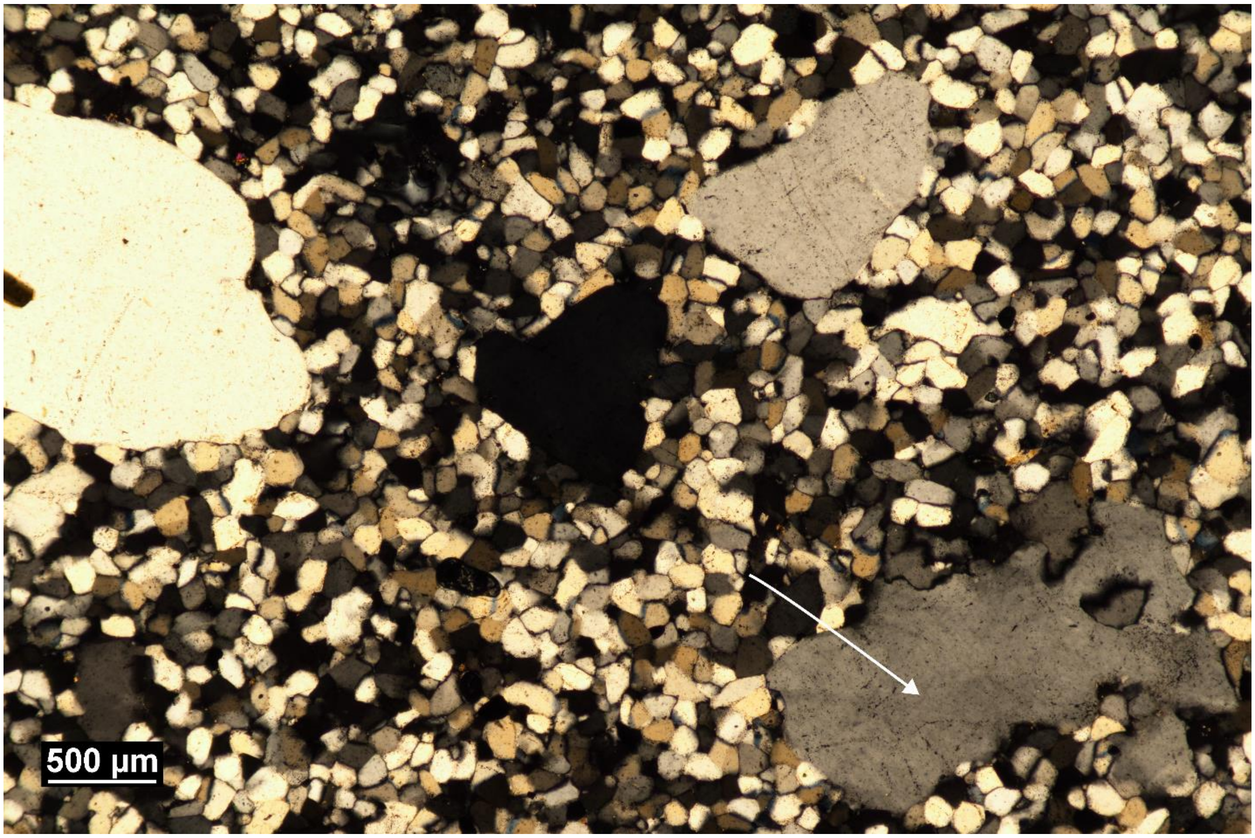


**Figure 13.** Grain boundary migration in deformation band Harding Sandstone.

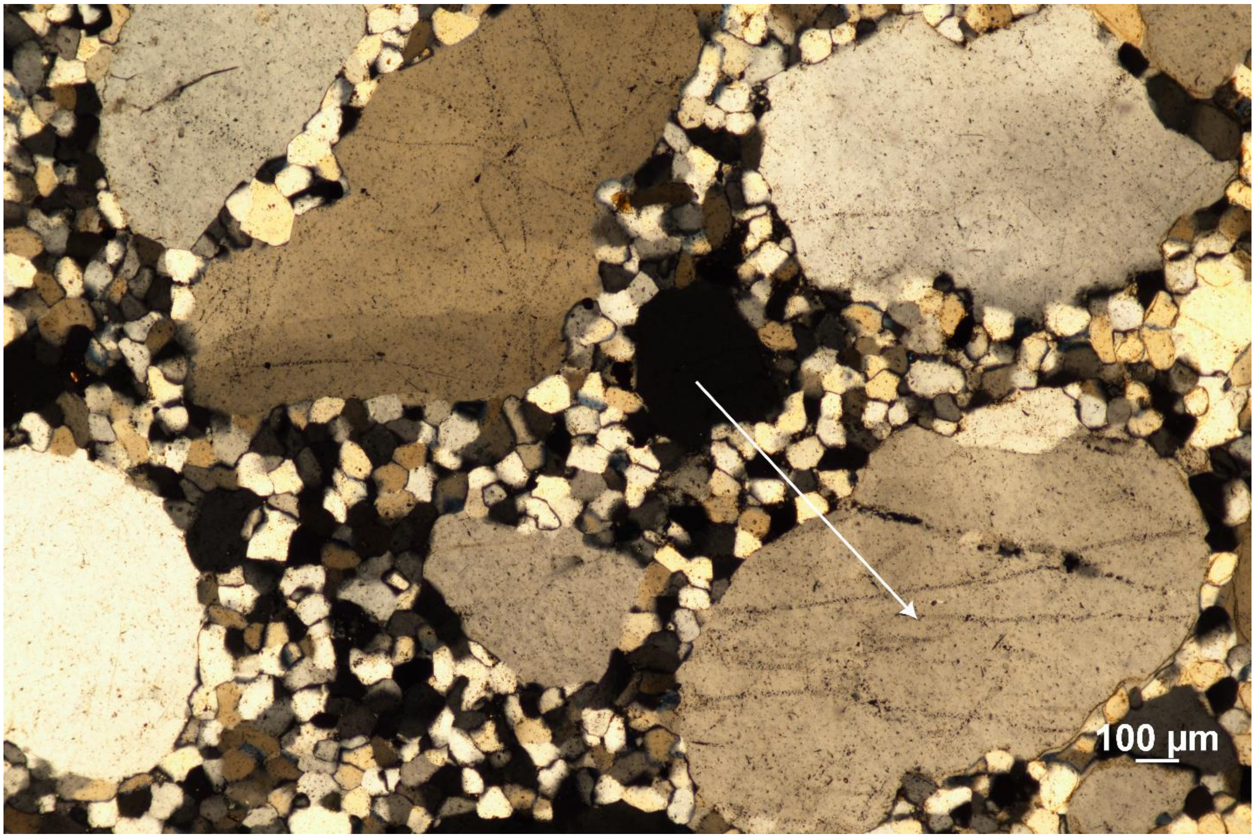


**Figure 14.** Trails of fluid inclusions in silicified Harding sample.

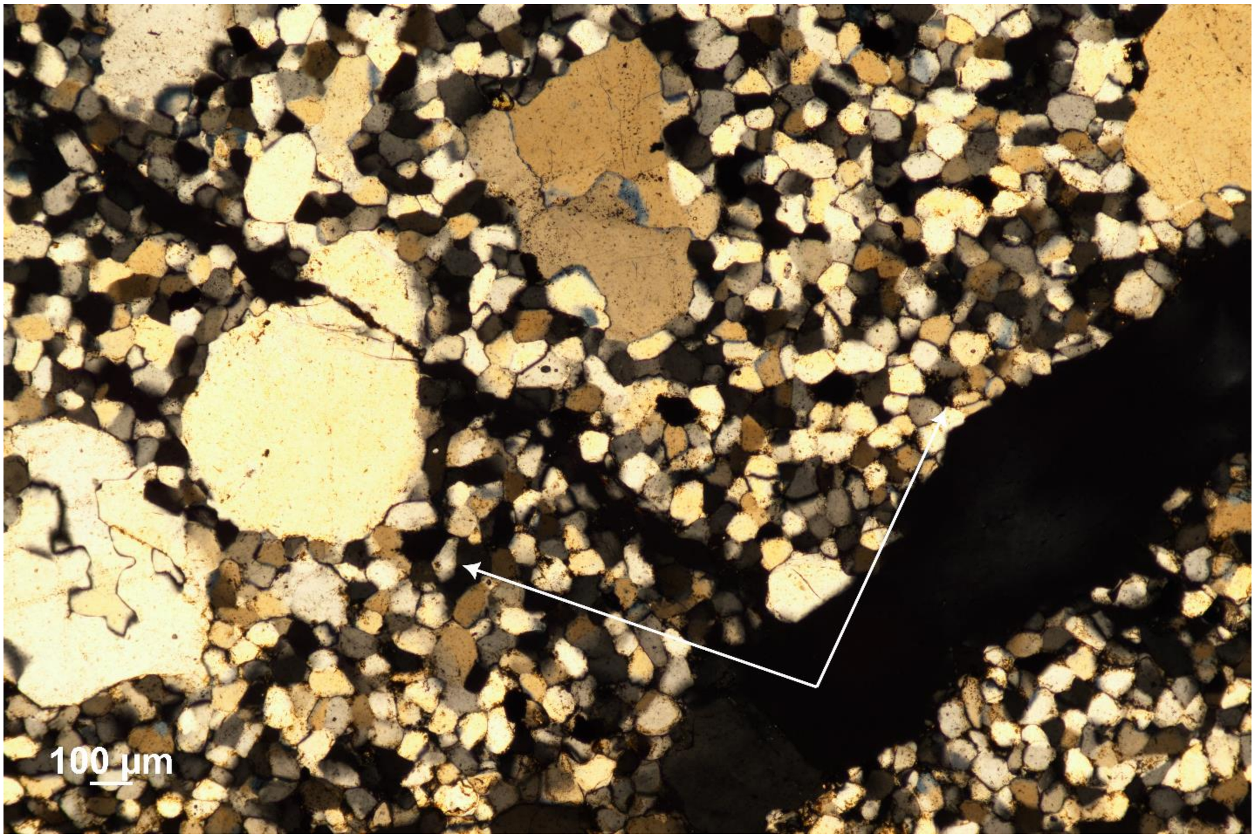


**Figure 15.** Polycrystalline quartz with irregular grain boundaries in silicified Harding formed in response to grain boundary migration recrystallisation.

**Figure 16.** Outcrop of Fremont exposure within the Mixing Bowl.

**Figure 17.** Exposure of the reddish Fountain Formation.

**Figure 18.** Extensive exposure of the Ralston Creek Formation.

**Figure 19.** Weathered, broken chunks of the Ralston Creek outcrop.

**Figure 20.** Extensively weathered exposure of the Morrison Formation.

**Figure 21.** Greenish soil around the Morrison Formation is due to weathering of the shaly part of the formation.

**Figure 22.** Northwest dipping beds of Dakota Sandstone.

# CHAPTER FOUR

## Structural Units

### 4.1 Faults

The rocks in the study area are deformed by two generations of thrust faults (Fig. 35). One of the faults cuts through the rocks of the study area from the southern part towards the northern extremities. This fault cuts through the Proterozoic Basement Gneiss, the Ordovician Harding, and the Pennsylvanian Fountain Formation. The second thrust fault in the study area traverses from the east to the west, cutting through rocks of the Proterozoic Basement Gneisses, Ordovician Harding, Pennsylvanian Fountain, Jurassic Ralston Creek, and Jurassic Morisson Formation. The N-S trending thrust fault is abutted by the E-W trending thrust fault in the northern segment of the study area. The N-S trending thrust fault has caused shearing and brecciation of Harding Sandstone and the Basement rocks, especially at a key location where it exists as a fault contact between Harding, Manitou, and Basement. The presence of this fault was characterized by broken chucks of quarzitified Harding Sandstone scattered around within fault zones. These faults zones are characterized by sheared surfaces, slickensides and striations on the fault planes.

The E-W trendine thrust fault is a high angle, steeply dipping thrust fault which contributed to the uplifting of the extensive Precambrian Basement gneiss in the northern boundary of the study area (Fig. 24). At the far western end of the study area, this fault created a triple junction between the Basement, Harding, Ralston Creek, and Morrison Formations.

## 4.2 Unconformities

According to the tectonostratigraphy and juxtaposition relationship between the different Formation in the study area, the Cretaceous Dakota Sandstone, Jurassic Morisson Formation, and the Jurassic Ralston Creek Formation are all separated by disconformable contacts (fig. 34). In the far northwestern flank of the study area, there is an unusual contact between the Jurassic Ralston Creek rock unit and the Proterozoic Basement. This is only possible through the presence of an unconformity contact due to their age differences. This unconformity is very extensive and can be traced continuously from the far eastern portion of the study area to the western part. It is represented by a purple wiggly line on the map and tectonostratigraphic section. Going downwards in the stratigraphic column, the contacts between the Pennsylvanian Fountain Formation and Ordovician Fremont Formation, Pennsylvanian Fountain Formation and Ordovician Harding Formation, and lastly the Pennsylvanian Fountain and Proterozoic Basement can also be described to be related to another single unconformity contact, represented by a yellow wiggly line on the map. Therefore, there are two general types of unconformity contacts in the study area of varying ages. The existence of a triple contact between the Proterozoic Basement, Jurassic Ralston Creek Formation and Pennsylvanian Fountain Formation depicts a situation where a more recent unconformity cuts through another unconformity.

### 4.3 Tectonostratigraphic and Juxtaposition Relationships

The Proterozoic basement rocks are mapped in the central and northernmost parts of the study area. In the northernmost parts of the study area, gneiss exposures are seen to be in fault contact with Formations like Harding, Ralston Creek and Morrison. The Cretaceous Dakota units bound the study area majorly in the northwestern, western, through the southern and then the extreme eastern side of the study area. A normal stratigraphic or depositional contact was observed between the Dakota, Morrison, and Ralston creek units, while other rock units are either unconformably related or in fault contact with each other. There is a nonconformable relationship between the Harding and the Basement in the northern and central region of the Mixing Bowl.

#### 4.3a Basement/Harding/Fountain contact

In the study area, the Harding, Basement and Fountain are found to be in non-conformable or fault contact with each other. In the norther part of the study area, the stratigraphy is seen to have been tectonically tilted so much so that the basement is pushed upwards by the thrust fault above both the undeformed Harding and Fountain Formation which are already separated by an older generation of unconformity (fig. 24). This same thrust fault has been interpreted to be responsible for the triple contact between Fountain, Harding, and Basement at the eastern portion of the map.

The central portion of the Mixing Bowl marks another location where a fault contact is observed between Harding and Basement rock units, but not Fountain (fig. 25). This is interpreted to be the thrust fault which traverses the study area from the northern through the southern part. A clear depiction of this is found in a critical location where an exposure of

Harding is in fault contact with sheared Manitou and Basement. This Basement/Harding contact is characterized by the presence of fault surfaces, slickensides and slickenlines. Rocks found within the vicinity of this contact are sheared and broken into chunks, giving rise to breccias, cataclasites and tectonic quarzite. Orientation of this thrust fault within tectonic quartzite is 79°/345°. Also observed within the central part of the Mixing Bowl is a nonconformable contact between the Fountain and the Basement units. This angular unconformity is the older of the two generations of unconformities observed. The plane of unconformity has an orientation of about 05°/278° in one location. Numerous measurements of orientation were collected in so many localities where this unconformity was seen and recorded within the study area.

### 4.3b. Basement/Morrison/Ralston Creek Contact

At the far northwestern corner of the map, the Basement was observed to be in fault contact with the younger Jurassic Morrison Formation and Ralston creek, thereby creating a triple junction contact (Fig. 26). The fault is oriented W255 at this point of contact. A second generation of unconformity was observed between Ralston Creek and Basement (fig. 27), in the central-southern portion of the study area. This angular unconformity depicted with a purple wiggly line is the youngest amongst the two unconformities. At a typical location in the western part of the map where this relationship was observed, the plane of unconformity has an orientation of 37°/046°. This unconformity leads to a Harding exposure, which is whitish and crystallized.

### 4.3c. Harding/Fremont Contact

There is an unconformity contact between the Harding and the Fremont rock units. Fremont was exposed in the form of small knobs and hills within the Mixing Bowl. It was observed that the orientation of the beds above the plane of contact is the same as the orientation of the beds below the contact. Fremont exposures were very limited and only seen in the central and northwestern parts of the study area. In a specific location where this contact relationship was clearly exposed, the orientation of the contact plane is 05°/324° (fig. 28). Fremont does not form any contact relationship with Basement anywhere in the field area.

### 4.3d. Harding/Fountain Unconformity

The first-generation angular unconformity clearly exists between the Harding and Fountain Formations (Fig. 29). This unconformity is represented on the map by a wiggly line in the eastern and western parts. Where this relationship is seen in the field, the Fountain is observed sitting in direct contact on top of the Harding Sandstone especially in the far northeastern quadrant of the map area, in association with the Laramide fault. At a particular location where this contact relationship is clearly observed, the orientation of the plane of unconformity is 25°/142°.

### 4.3e. Fremont/Fountain Contact

Only one type of contact exists between the Fremont and the Fountain Formation. These two rock units are separated by the first-generation angular unconformity. Good examples can be seen in the northwestern and central or slightly towards the western part of the Mixing Bowl (Fig. 30). The orientation of the plain of unconformity at this location where it is well represented is 12°/040°. Bedding attitudes dip between 10° and 20° towards the southeast along the contact where the Fountain Formation rests irregularly above the Fremont Formation. It was observed that some Fountain units were eroded in some sort of stream channel with conglomerate clasts scattered all over.

### 4.3f. Ralston Creek/Fountain Contact

The Ralston Creek Formation is unconformably positioned over the Fountain Formation (fig. 31). This unconformity in between the two Formation is a second-generation angular unconformity which is younger than the unconformity that separates the Fountain and the Fremont. Ralston Creek, wherever deformed, usually contains deformation bands and slickensides in it. The orientations of both units diverge by approximately 20° southwards along the unconformable contact in the eastern direction.

### 4.3g. Morrison/Ralston Creek

There is a depositional contact between the Morrison Formation and the Ralston creek Formation where the Morrison Formation lies conformably above the Ralston Creek Formation (fig. 32). This is a normal contact which is consistent with the stratigraphy of the Mixing Bowl that has been reported by previous workers. This contact is very visible and clear in some places but very obscure and less visible in so many localities in the study area. Where these contacts are unclear because of the weathering of the Morrison Formation, it was mapped as an inferred contact. Here, only signs of its presence are seen from the greenish color of the soil. At a particular location where the contact is very clear, the contact plane has an orientation of 23°/110°.

### 4.3h. Morrison/Dakota Sandstone Contact

An unconformity contact exists between the Morrison and the Dakota sandstone, and it is consistent with the depositional history of the Mixing Bowl. The Dakota Sandstone lies conformably above the Morrison Formation (Fig. 33). This contact is observed in several locations in the study area. Dakota has some deformation bands in it. There are Dakota exposures that have been weathered into vertical rectangular block of rocks. Fragments of Dakota materials which fell off the Dakota cliffs have obscured the Morrison/Dakota contacts in many localities; therefore, this depositional contact is not easily deciphered.

### 4.4 Structural Analysis

Two generations of thrust faults and unconformities are responsible for the complex juxtaposition relationship of the rock formations in the study area (Fig. 34). The study area is bounded to the east, south, and west by Cretaceous sedimentary units, while to the north, it is bounded by basement rocks. In the northern portion of the map, the thrust fault creates fault contact with Harding, Fountain, Ralston Creek, and Morrison Formations. In the central to southern parts of the map, there is a fault contact between the fault and just the Harding and sheared Manitou. The older and younger unconformities also form unconformity contacts either between Proterozoic units and Cretaceous units or just between Cretaceous Formations (Fig. 35).

Throughout the Mixing Bowl study area,1102 bedding plane orientation measurements were collected across the different Formations and localities using the FieldMove clino app. The stereonet in Fig. 36a, displays 250 bedding measurements of the Dakota Sandstone plotted as great circles. It can be observed from this figure that the beds of the Dakota Sandstone dip in all directions, but the dominant direction of the beds is towards the southeast. The minimum dip of the Dakota beds is 01° and the maximum dip is 86°.

Stereonet observation of the Fountain Formation displays 42 Fountain beds plotted as great circles (Fig. 36b). Almost all the beds in this Formation dip towards the north, east and south. Very few beds dip to the west. The dominant dip direction of the beds in the Fountain is towards the east, with a minimum dip angle of 02° and a maximum dip angle of 60°.

Stereonet observation of the Fremont shows 3 beds plotted as great circles (fig. 36c). All 3 Fremont beds dip roughly towards the north. Since most of the Fremont exposures mapped in the Mixing Bowl occur as small, rough hills and mounds, the orientation of their beds was difficult to measure and hence approximated using a clipboard. The dominant orientation of the Fremont beds is towards the north. The minimum dip of the beds is 20° and the maximum dip is 49°.

Stereonet observation of the Harding Sandstone shows 149 beds plotted as great circles (Fig. 36d). Beds of the Harding Sandstone dip in all directions. The most dominant dip direction is towards the east. The minimum dip angle of the Harding beds is 02° while the maximum dip is 33°.

Stereographic plots of Morrison beds display 137 bedding orientations plotted as great circles (Fig. 36e). These Morrison beds dip in all directions but dominantly towards the southeastern direction.  The minimum dip angle of the Morrison beds is 02° and the maximum dip angle is 58°.

Stereographic plots of the Ralston creek beds show 72 bedding orientation measurements plotted as great circles (Fig. 36f). The beds here dip dominantly towards the east and southeastern direction. Minimum dip angle of the beds is 02° and the maximum dip angle is 50°.

Deformation band orientation measurements were collected in the Harding Sandstone. About 315 deformation bands were plotted on a stereonet as great circles (Fig. 37a). Most of the deformation bands dip to the east just as the host Harding Sandstone beds. The minimum dip of the deformation bands in 01° and the maximum dip is 89°. To get the dominant direction in which the deformation bands are striking, their azimuths were plotted using a rose diagram (Fig. 37c). From this diagram, it can be interpreted that the principal deformation band direction is trending from NE-SW, and minor deformation bands direction are NW-SE and NNE-SSW. The dominant NE-SW orientation of the deformation bands is in line with the orientation of the extensive second generation thrust fault.

About 25 fault planes from all the Formations in the Mixing Bowl were measured. These readings have been plotted in a stereonet as great circles (Fig. 38a). The faults dip in all directions probably because of multiple orogenic episodes in the study area. Fault planes associated with the first generation of thrust faults and second generation thrust faults were plotted on a rose diagram. The principal orientation of the first generation thrust fault is N-S and NNW-SSE (fig. 38b), while the principal orientation of the second generation thrust fault is NE-SW (fig. 38c).

Joint measurements from the Precambrian basement and Ralston creek have been plotted on a stereonet. The total number of joints analyzed is 49. The dominant dip direction of these joints plotted as great circle is to the east (Fig. 39a). The dominant orientation of the joints in the Mixing Bowl is NE-SW and NNE-SSW to some extent (Fig. 39b).

Evidence of folding was observed in a locality in the southeastern part of the Mixing Bowl within the Dakota Sandstone. Here, Dakota exposure is found with beds dipping in opposite directions. These beds are the limbs of the fold. The orientation of the SE dipping limb is 27°/007° and the orientation of the SW dipping limb is 33°/249°.

### 4.4a. Pretilt Orientation of Beds below Unconformities

Stereographic rotation of beds below the plane of unconformities is achieved in two ways. Figure 36 represents the plot of all bedding orientations for each individual formation as great circle. The bedding from the different formations is oriented in varying directions. The strike and dip values representing the average bedding orientation for Dakota, Fountain, Fremont, Harding, Morrison, and Ralston Creek Formations are recorded in Tab. (1) and Fig. (40). The tectonostratigraphy and juxtaposition relationship observed in the study area through detailed structural mapping reveals that the Harding Formation, Fremont Formation, and the Fountain Formation all occur in the Mixing Bowl as beds below either the first or second generation of unconformities.

The result after unfolding and rotating these beds are shown in Fig. (41) and Tab. (2). The Harding, Fremont and Fountain beds have orientations of 203°/7°/W, 253°/36°/N and 316°/5°/E respectively.  These can be interpreted as the orientation of the beds before deformation and tectonic tilting and the creation of unconformities. Planar orientation of beds above and below both angular unconformities measured directly in the field have been rotated sterographically. The Ralston Creek, Fountain, Fremont, and Harding Formations form beds found above and below the different unconfrmities. The result is a distribution of pre-unconformity Harding or the orientation of the Harding beds before tilting plotted on a stereonet (Fig. 42).

### 4.4b. Fault Damage Zones Analysis in the Mixing Bowl

A fault has two major components which are the fault core and the surrounding damage zone (Chester et al., 1993; Caine et al., 1996; Berg and Skar, 2005). Moving from the fault core into the damage zone and then host rock, the intensity of deformation decreases (Torabi et al., 2020). The damage zone of a fault refers to the deformed outer volume of rock surrounding the fault core. It may contain fractures, minor faults, fault rocks and deformation bands (e.g., Torabi et al., 2020; Torabi & Berg, 2011; Berg & Skar, 2005; Faulkner et al., 2010; Billi et al., 2003). In this thesis, I have investigated the permeability and how it varies within the Harding Sandstone in the mixing bowl study area.

Three groups of data were used based on the locations of the different types of deformation withing the Harding Sandstones in the study area and are saved in three different data files. These Harding Sandstone types are deformation band Harding, quartzitified Harding and the undeformed Harding. The data are made up of permeability measurements (mD), distance or increment (m) readings between sampling points taken from the fault core outwards towards the damage zone and host rock for both the deformation band Harding and the quartzitified Harding. But for the undeformed Harding, permeability measurements were taken with distance along the stratigraphy from top to bottom. The variables measured, which are permeability and increment, all fall under the category of ratio data. These data can also be described as open data because the data are not constrained by the measurement system. The same size used for this project is approximately 200 samples across all data files.

I tested for normality quantitatively and by visualizing the distribution using the stripchart () function in R studio software. The data are asymmetrically distributed and mostly right skewed. I also tested for normality using the Shapiro-Wilk test (Shapiro.test()) in R studio interface. From the Shapiro test, the following p-values for the permeabilities of the different Harding types were obtained. The deformation band Harding has a p-value of < 2.2e-16, quartzitified Harding has a p- value of < 1.341e-08, and the undeformed Harding has a p-value of < 3.41e-13. These p-values are extremely small and are evidence that all three data from all

Harding Sandstone types are not normally distributed.

A T-test was conducted on each Harding Sandstone to get their estimate and confidence interval using the t.test () function in R. The mean permeability of deformation bands Harding Sandstone in the study area is 70630.06 mD (95% C.I.: 23118.13 – 118142 mD). The mean permeability of quarzitified bands Harding Sandstone in the study area is 73875.05 mD (95% C.I.: 15126.2 – 132623.9 mD). The mean permeability of the undeformed Harding Sandstone in the study area is 1415189 mD (95% C.I.: - 472470.8 – 3302848.7 mD). The results are the t-test approach show that the undeformed Harding Sandstone is the most permeable with a mean permeability of 1415189 mD, and the deformation band Harding Sandstone is the least permeable. This is consistent with the work of Fossen and Bale (2007), who reported that deformation bands when present in porous sandstones tend to reduce permeability in their host rocks.


**Figure 23.** Precambrian Basement, Ordovician Harding, and Fountain units in fault and unconformable contact.

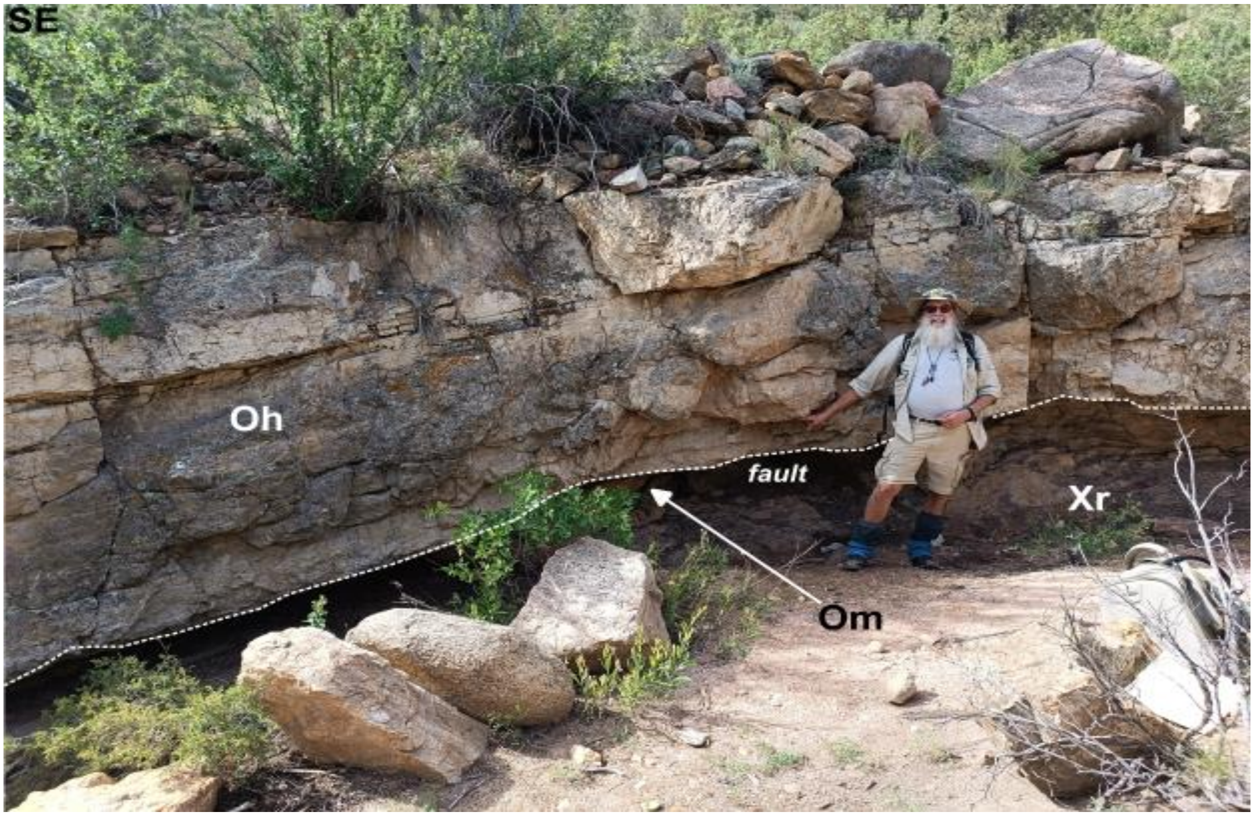


**Figure 24.** Fault contact between Ordovician Harding, Precambrian Basement, and sheared Manitou units.

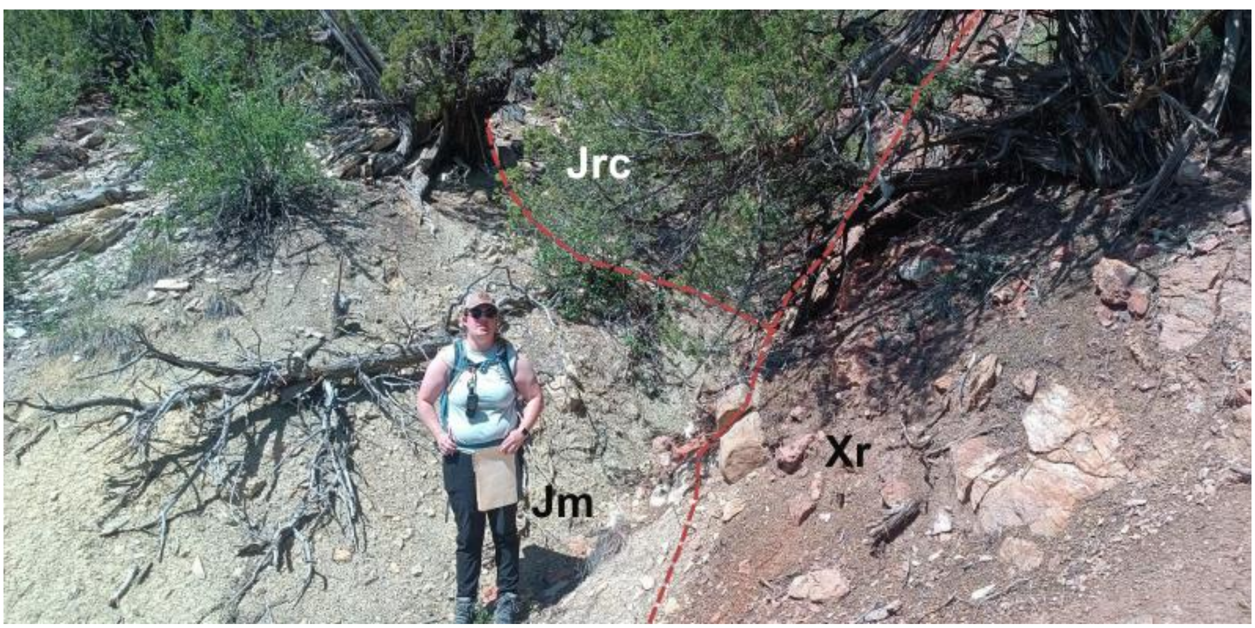


**Figure 25.** Triple-junction contact between Precambrian Basement, Jurassic Morrison, and a nearby Jurassic Ralston Creek Exposure.

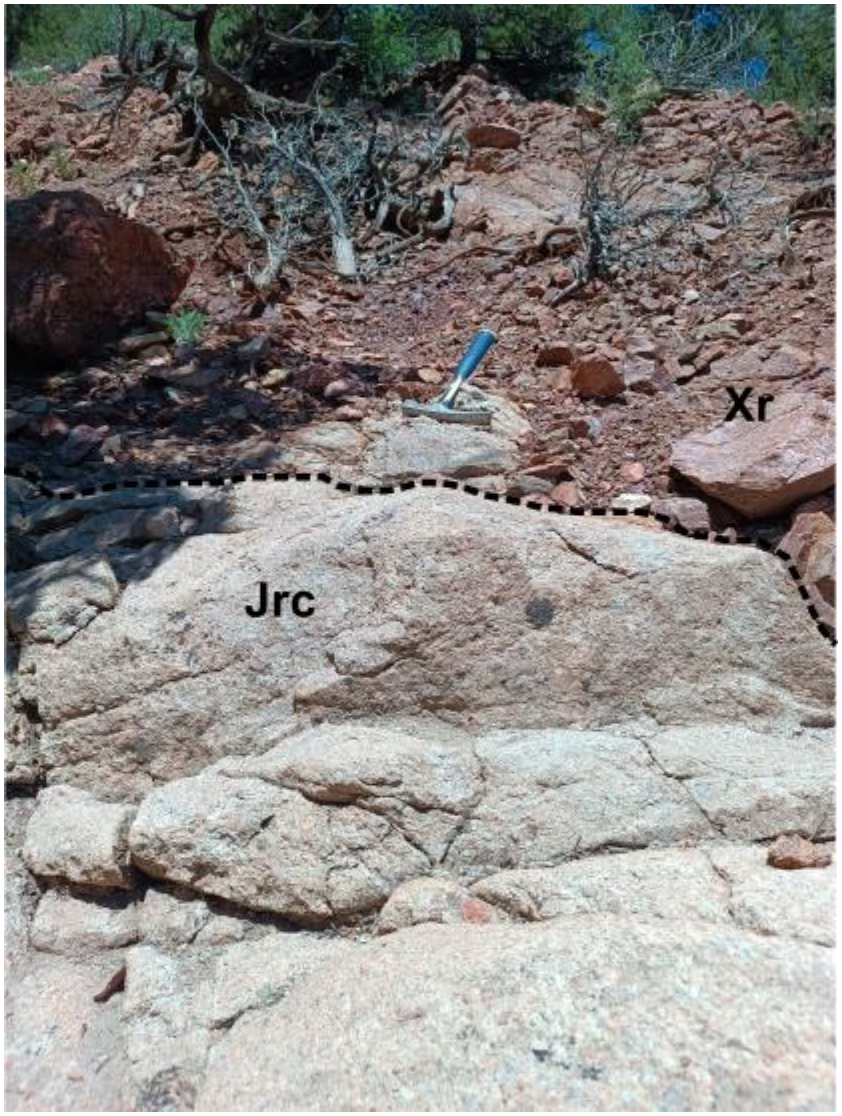


**Figure 26.** Unconformity between the Precambrian Basement and the Jurassic Ralston Creek sandstone.

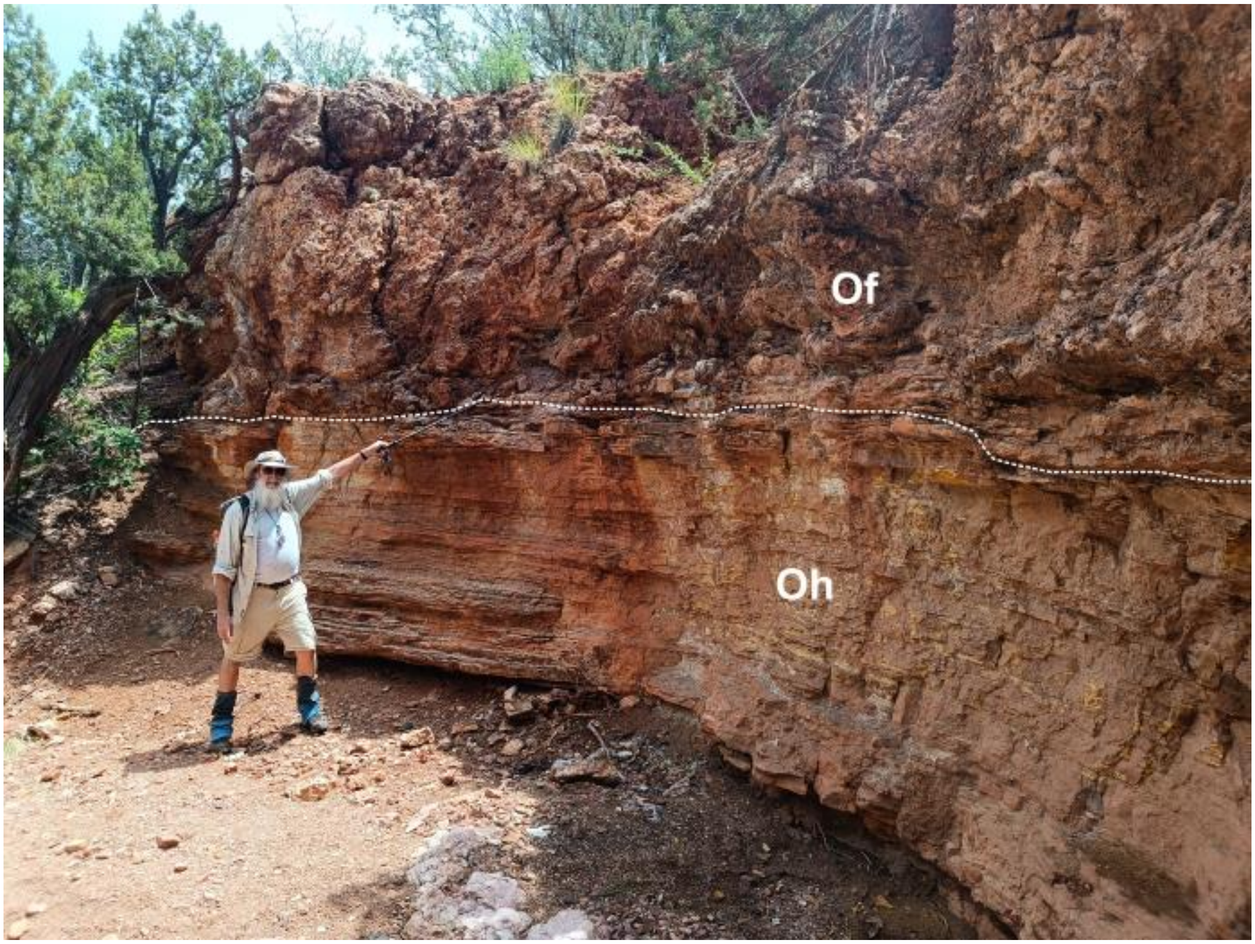


**Figure 27.** Unconformable contact between Ordovician Harding and Ordovician Fremont Formations.


**Figure 28.** Unconformable contact between Pennsylvanian Fountain Formation and Ordovician Harding sandstone. (a) Undeformed Harding sandstone and Fountain contact. (b) Contact between deformation bands Harding sandstone and Fountain Formation.

**Figure 29.** Unconformity between Ordovician Fremont and Pennsylvanian Fountain Formation.

**Figure 30.** Unconformity between the Jurassic Ralston Creek and Pennsylvanian Fountain Formation.

**Figure 31.** Depositional contact between the Jurassic Morrison and Jurassic Ralston Creek Formation.

**Figure 32.** Depositional contact between the Morrison Formation and Dakota sandstone.

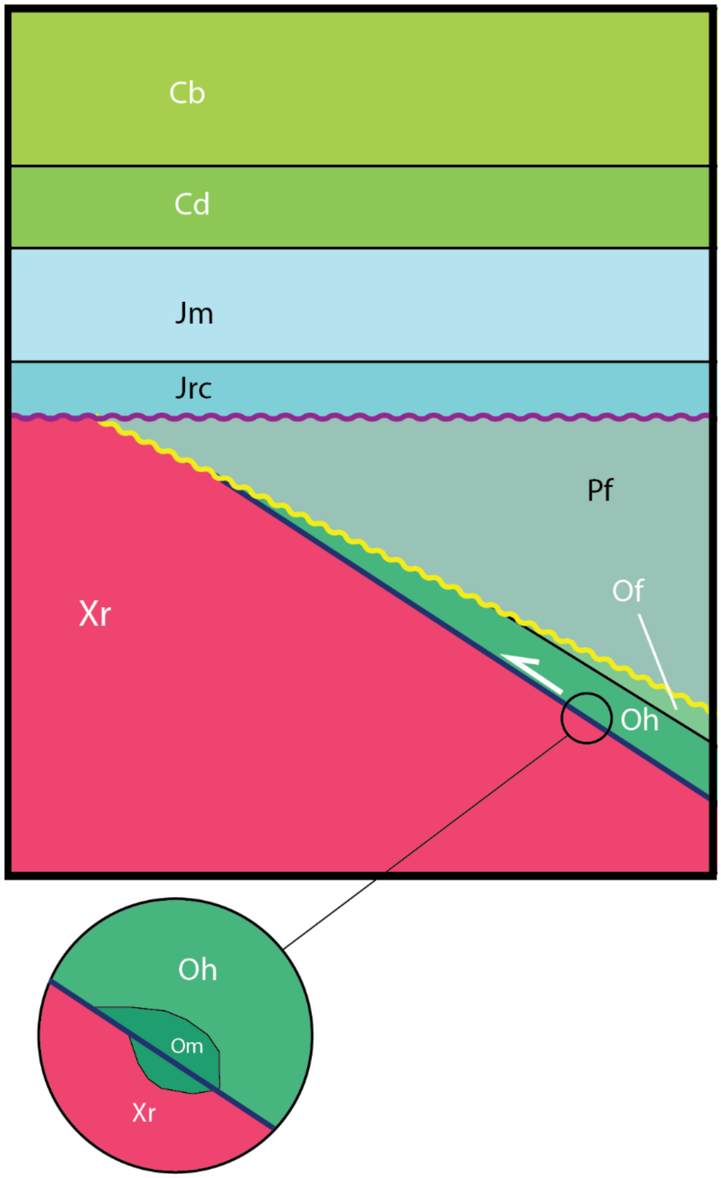


**Figure 33.** Tectonostratigraphy of the study area.

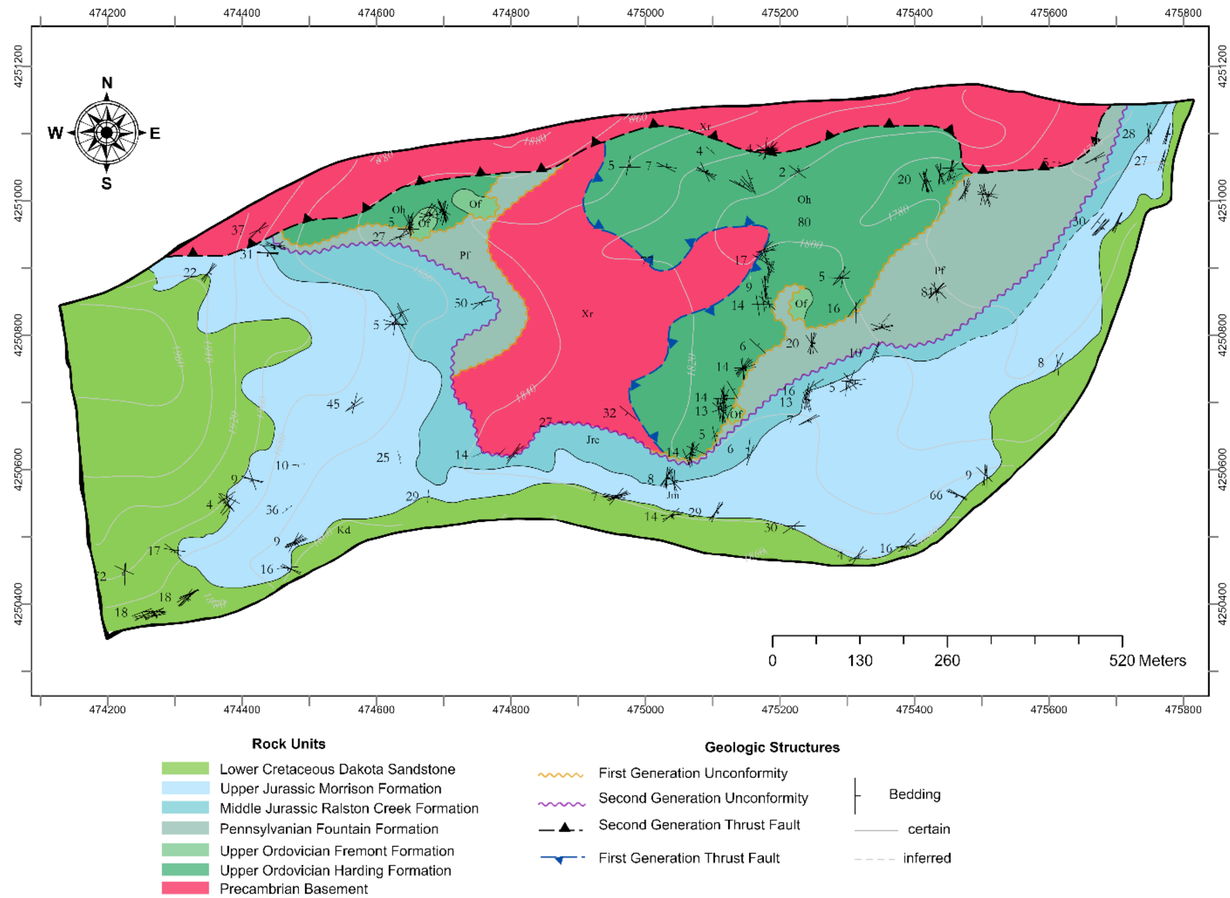


**Figure 34.** Structural map of the study area.

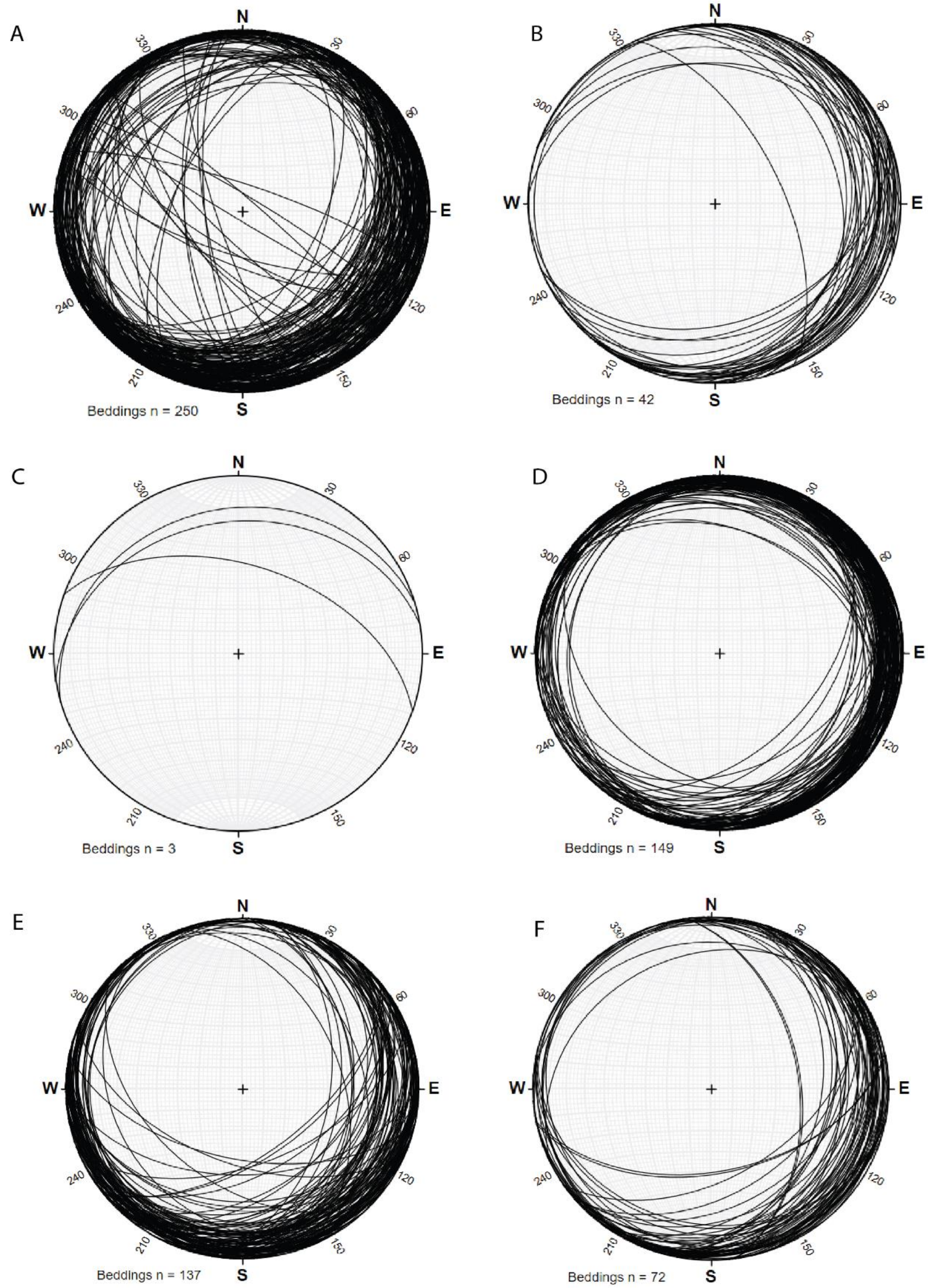


**Figure 35.** Plot of bedding orientation of all Formations as great circles. (a) Dakota Sandstone. (b) Fountain Formation. (c) Ordovician Fremont Formation. (d) Ordovician Harding. (e) Jurassic Morrison Formation (f) Jurassic Ralston Creek.

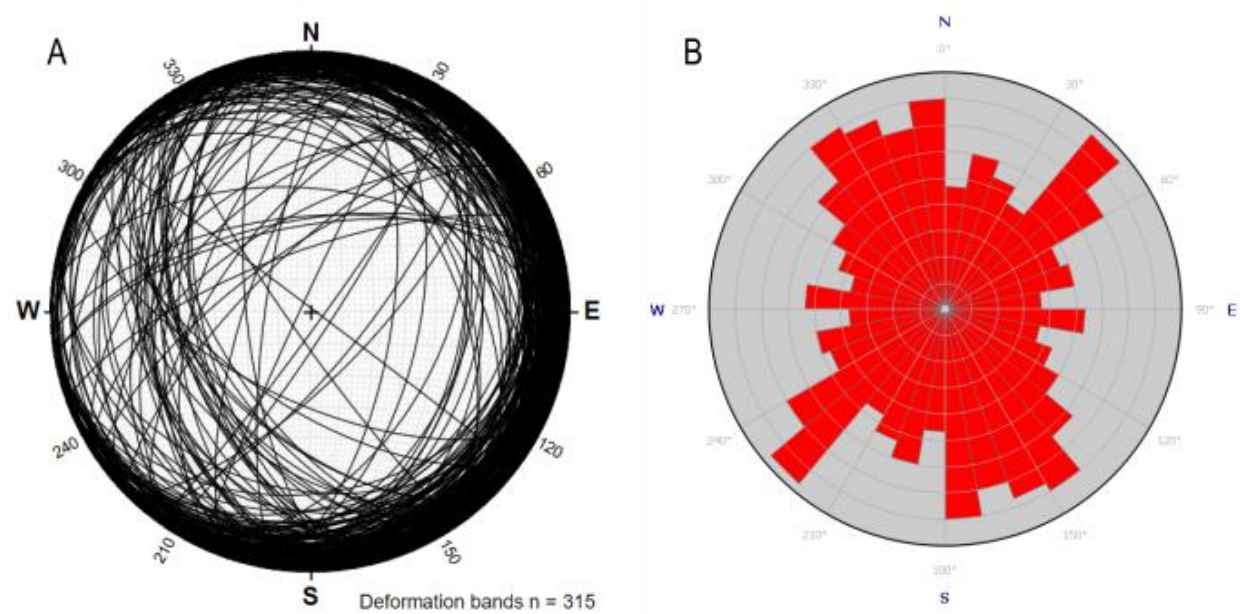


**Figure 36.** Stereographic plots and rose diagram of all Harding deformation bands in the study area. (a) Deformation bands plotted as great circle. (b) Rose plot showing the dominant deformation bands orientation.

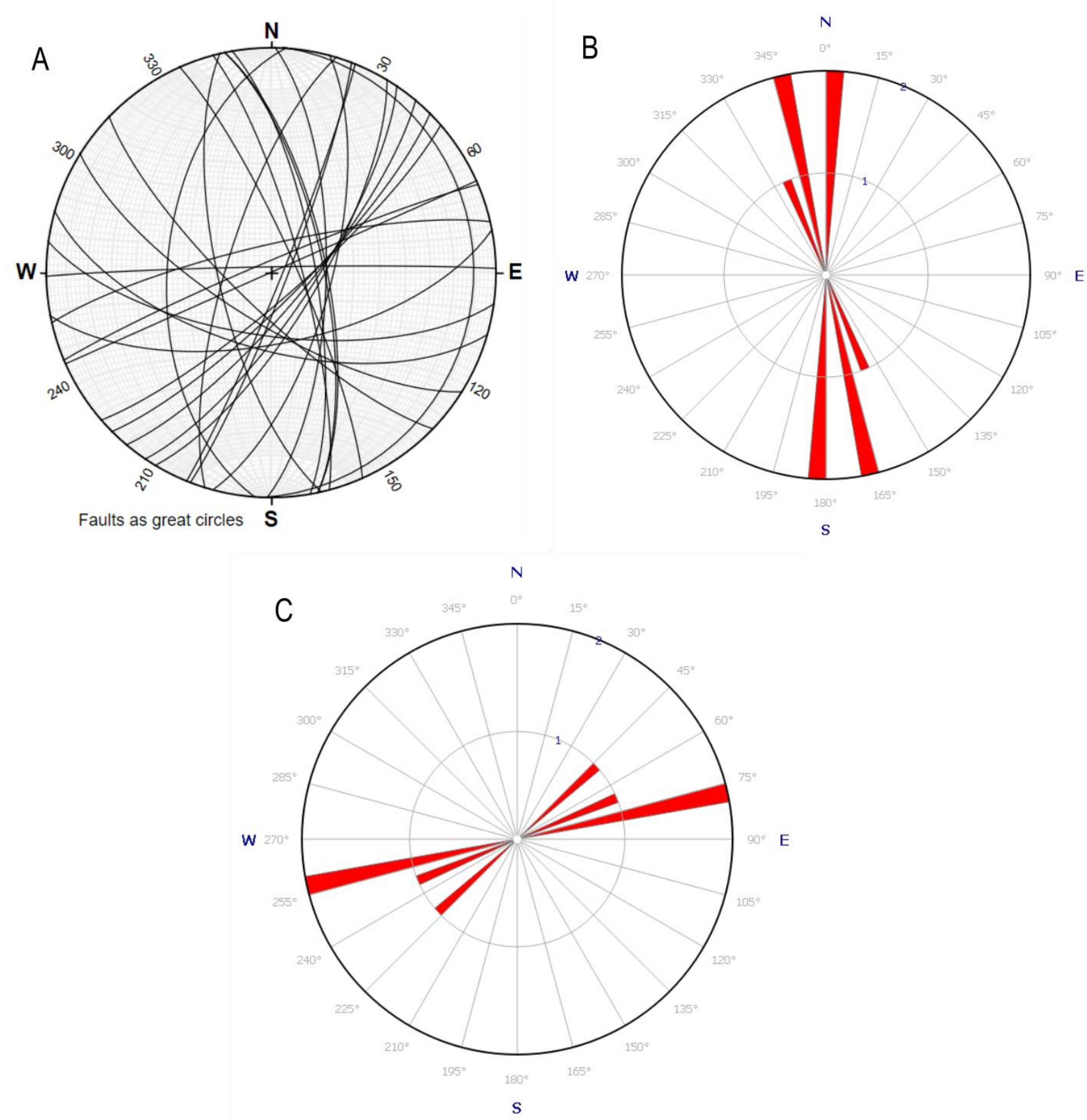


**Figure 37.** (a) All major and minor fault planes plotted as great circles. (b) Rose plots showing the major orientation direction of the first generation of thrust fault planes. (c) Rose plots showing the major orientation of the second generation of fault planes.

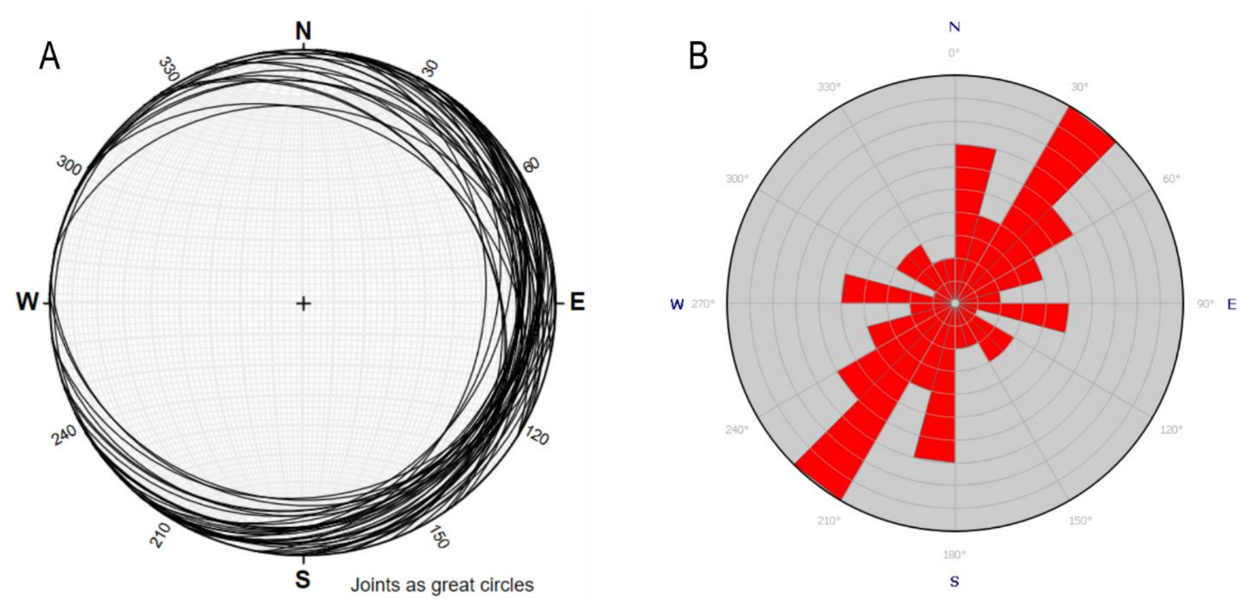


**Figure 38.** (a) Joint planes on exposed Gneiss and Ralston Creek surfaces plotted as great circles. (b) Rose diagram of these joints.

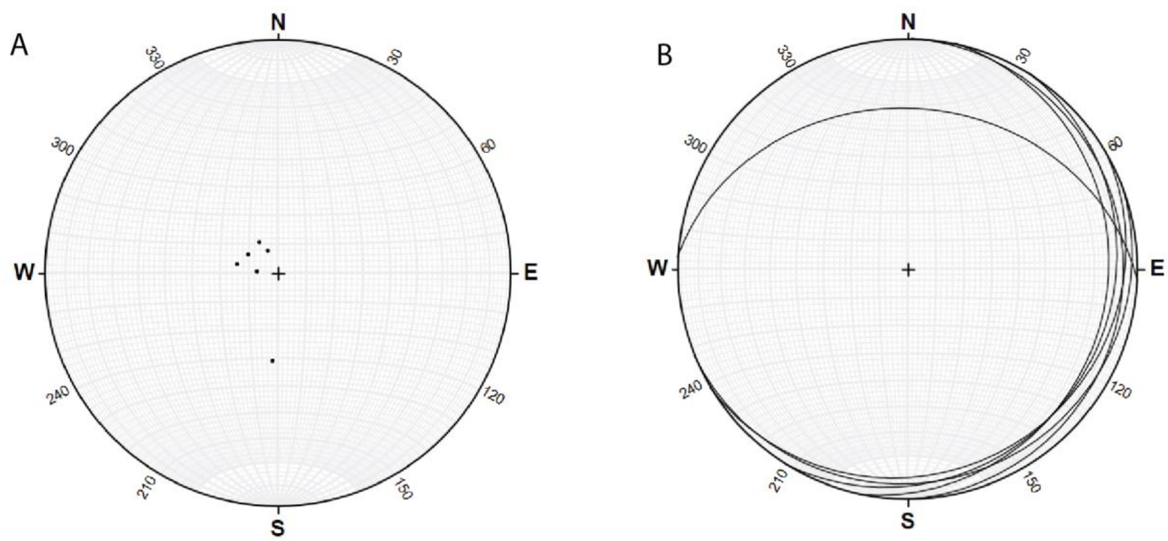


**Figure 39.** Average bedding orientation measurements from all sedimentary units plotted on Stereonets. (a) Plotted as poles. (B) Plotted as great circles.

**Table 1.** Average bedding readings from different rock units.

| Formation | Average Trend/Plunge | Average Strike/Dip/Dip Direction |
|---|---|---|
| Dakota | 338°/82° | 068°/8°/S |
| Fountain | 282°/76° | 012°/14°/E |
| Fremont | 183°/59° | 273°/31°/N |
| Harding | 271°/83° | 001°/7°/E |
| Morrison | 329°/78° | 059°/12°/S |
| Ralston | 302°/78° | 032°/12°/E |

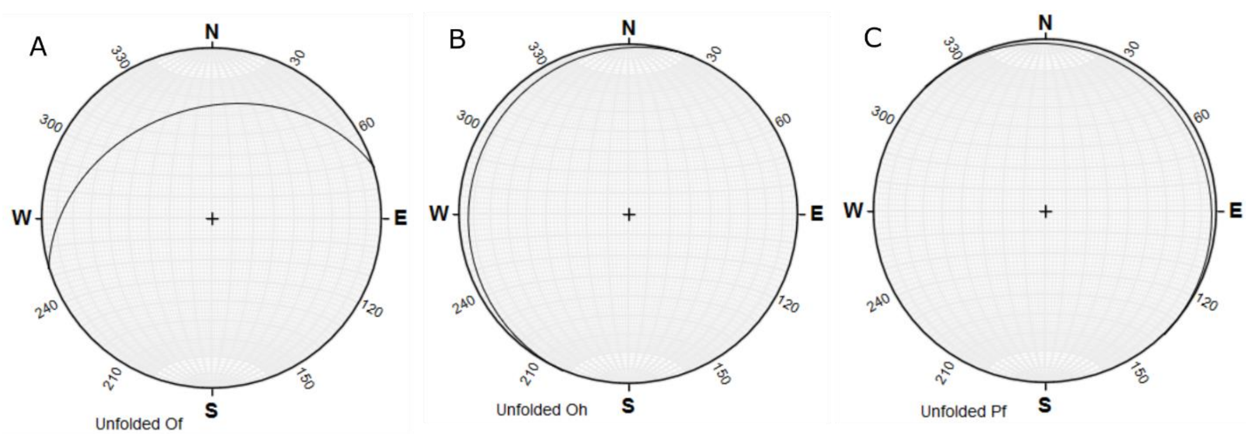


**Figure 40.** Stereonets for unfolding and rotating beds below the unconformities. (a) Unfolded Fremont bed. (b) Unfolded Harding bed. (c) Unfolded Fountain bed.

**Table 2.** Orientation values of Beds below unconformities after unfolding and rotation.

| Unconformity | Rotated Lower beds | Orientation after Rotation |
|---|---|---|
| Fountain/Harding | Harding | 203°/7°/W |
| Fountain/Fremont | Fremont | 253°/36°/N |
| Ralston Creek/Fountain | Fountain | 316°/5°/E |

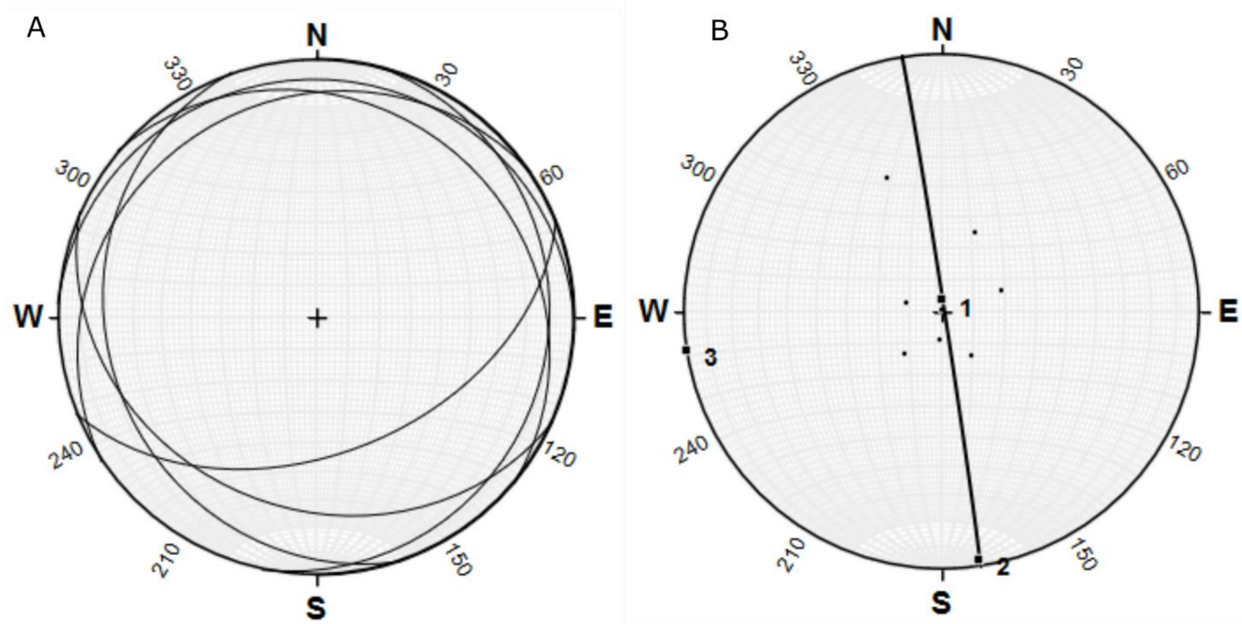


**Figure 41.** (a) Pretilt Harding beds orientation plotted as great circle. (b) Poles to Harding beds with best fit great circle.

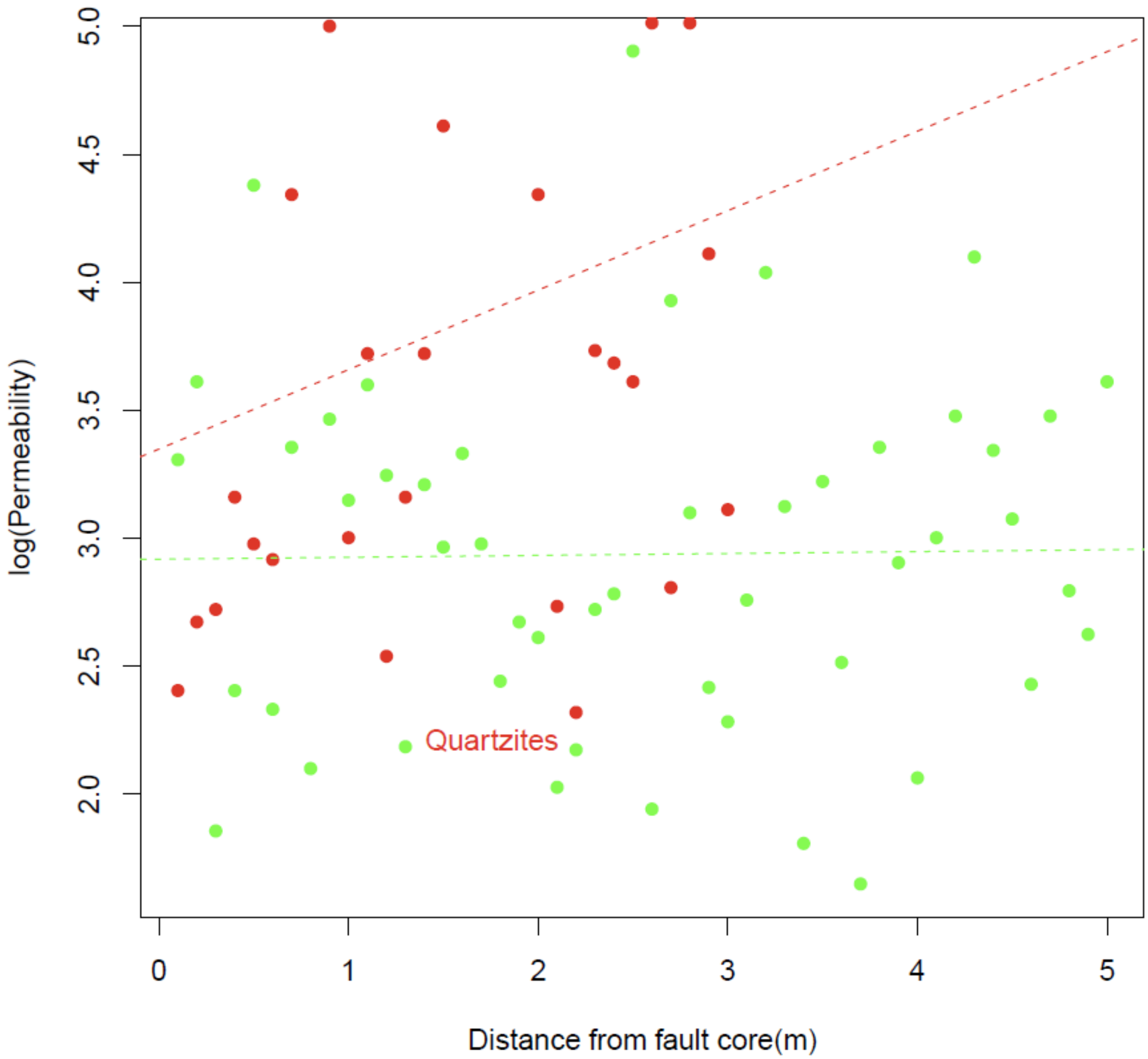


**Figure 42.** Bivariate plot of log (permeability) vs distance from fault core depicting a non-linear correlation in the data. Green points = deformation band Harding Sandstone; Red points = silicified Harding sandstone.

# CHAPTER FIVE

## Discussion

Through lithological and structural mapping of the CCE, rocks ranging in age from Precambrian to Cenozoic have been described. The rock types found in the study area are metamorphic rocks like gneiss which represent the basement component of the tectonics and sedimentary rock units representing the cover. Sequence of sedimentary rock formations such as the Lower Ordovician Manitou, Middle Ordovician Harding, Upper Ordovician Fremont, Pennsylvanian Fountain, Middle Jurassic Ralston Creek, Upper Jurassic Morrison, and the Dakota Sandstone have been observed and documented at the field site. The juxtaposition relationship between the different rock units revealed the presence of not just conformable contacts, but key beds separated by multiple generations of angular unconformities and thrust faults that are related to the Ancestral Rocky Mountain and Laramide orogenies. Comparing the permeabilities between the different Harding types found in association with these generations of faults depicts how the porosity and permeability of rocks containing deformation bands is reduced to a larger extent compared to rocks without deformation bands.

Previous work in the CCE, especially the work of Anlian (2017), reported the presence of the Laramide orogeny related structures in the Mixing Bowl, but results from current field mapping exercise provides evidence to show that rocks in the area were actually affected by two orogenic episodes which are the Ancestral Rocky Mountain orogeny and the Laramide orogeny and these orogenies resulted to the development of two generations of thrust faults. The two generations of faults are characterized by deformed rock types, especially from the Harding Formation. Silicified rocks in the damaged zone of the first generation thrust fault serves as evidence of the Ancestral Rocky Mountain orogeny. The damage zone of the Laramide fault is interpreted to be characterized by the presence of deformations bands, especially in areas where it cuts through the Harding Sandstone.

The response of the Harding Sandstone to the movements related to the Ancestral faults is quite different from that of the Laramide. Here, local fault-related metamorphism may have transformed the Harding Sandstones to silicified fault rock within its damage zones. These two major faults were mapped by taking GPS readings at points where they were observed. The Ancestral Rocky Mountain thrust fault runs through the central portion of the study area from South to North where it is truncated by the younger Laramide thrust fault. A clear cross-cutting relationship is observed in this northern part of the study area. Traversing east-west along the Laramide faults in the northernmost portions of the map area provides evidence of Precambrian Basement upliftment.

Structures that are associated to the late Paleozoic era Ancestral Rocky mountain orogeny are very difficult to interpret because of Mesozoic and Cenozoic structural overprinting (e.g., DeVoto, 1980; Tweto, 1980; Weimer, 1980; Lindsey et al., 1983; Hoy & Ridgway, 2002; Sweet & Soreghan, 2010; Soreghan et al., 2012; Chapin et al., 2014). Many studies have confirmed that Ancestral Rocky Mountain structures are compatible with NE-SW directed intraplate shortening (Ye et al., 1996; Hoy and Ridgway, 2002; Thomas, 2007; Sweet and Soreghan, 2010; Leary et al., 2017; Sweet et al., 2021). To test for this, structural analysis was conducted on the various kinds of structures found within the study area. These structures are beddings, fault and fault planes, slickenlines, slickensides, deformation bands, joints and folds. A total of 1102 bedding measurements were taken across all the various Formations in the Mixing Bowl. Plotting these bedding readings on stereonets reveals that they dip in almost all directions. They dip to the east and southeast to a larger extent and in some cases to the west and north. The maximum dip angle is about 86° and this was observed in the Dakota beds (Fig. 36a).

Interpreting the orientation of brittle structures like faults and joints observed in the study area by plotting them on a rose diagram reveals that the faults planes associated with the first generation thrust fault are predominantly oriented in the NNW-SSE and N-S directions. This first generation thrust fault can be interpreted to be related to the Ancestral Rocky mountain orogeny because the block uplifts associated with Ancestral Rocky Mountains are oriented to the northwest (Haun & Kent, 1965; Sweet & Soreghan, 2010). Fault planes associated with the second generation of thrust fault plotted of a rose diagram displayed a preferred orientation towards the NE-SW direction. This thrust fault can be interpreted to have originated from the Laramide orogeny. The dominant orientation of joints measured is quite different from what is obtained from the faults. The joints are aligned in a NE-SW and NNE-SSW direction. The reason for this disparity might be because the joints encountered in the study area are mostly restricted to the Precambrian basement gneiss and the Ralston Creek Formation while evidence of faulting is seen in the Harding Formation.

Found associated to fault planes are structures that portray the movement within faults and direction of slip. These are the slickensides and slickelines. Orientations of slickenlines from fault planes, especially those within the damage zone of the quarzitified Harding sandstones, are plotted on a stereonet. Contouring these plots revealed that the axis of compression to be approximately NNW-SSE. Slickenlines are not the only structural feature associated with the fault damage zone. Almost all deformation bands Harding Sandstones associated with Laramide faults have deformation bands within damage zones. Deformation bands are tabular strain-localization structures that develop in very porous rocks and sediments as a result of grain breaking or reorganization (Torabi et al., 2020). According to Fossen and Bale (2007), they can be found as individual structures, occurring together as clusters and in fault damage zones. The orientation of deformation bands plotted on a stereonet reveals an easterly dipping direction, with the strikes orienting in a NE-SW and NNE-SSW direction as depicted on the rose diagram. This is consistent with the results of Bump & Davis (2003), who through interpretation of outcrop-scale structures like mesoscopic faults and deformation bands in Colorado and Utah reveals that there are two groups of Laramide uplifts, one with evidence of NW-SE contraction and the other with NE-SW directed compressive stress.

Both Ancestral Rocky Mountain and Laramide Orogenic deformations are associated with block uplifts. One area where this uplift is observed in association with a fault is at the northern part of the study area where Precambrian Basement rocks have been thrust upwards on Harding Sandstone along a fault. According to Kluth & Coney (1981), evidence for these uplifts is deduced from unconformities and deposition of coarse, arkosic sediments eroded from them. The first-generation unconformity symbolized by yellow/orange wiggly lines (Fig. 35) that exists between the Fountain Formation and the Harding Sandstone in the western and northeastern parts of the study area provides clear evidence of the Ancestral Rockies Orogeny.

The structural rotation of intraformational unconformities in proximal basin deposits occurs during deposition, therefore basin-margin deformation can be understood by analyzing the final geometric orientation of these rotated unconformities (e.g., DeCelles et al., 1993; Vergés et al., 1996; Ridgway et al., 1997; Hoy & Ridgway, 2002). Unconformities and sedimentary rock distributions have been used to show that the Wet Mountains, Front Range, and southern Sangre de Cristo arches were uplifted in the Pennsylvanian by the Ancestral Rocky Mountain orogeny (DeVoto, 1980; Tweto,1980; Kluth and Coney, 1981). Because rock units in the Mixing Bowl have beds that are separated by either of the two generations of unconformities, the original orientation of all the beds below the unconformities was determined using stereonets. Results from this pre-tilt analysis show that before deformation, the Harding Sandstone beds dip to the west, the Fountain beds dip to the east and the Fremont beds to the north. So, the Ancestral Rockies and Laramide orogeny can be interpreted to be responsible for the re-orientation of these beds from their initial orientations to their present geometry. Stereographic projection (Fig. 42) reveals that beds of the Harding Sandstone have been folded with fold axis oriented in a NNW-SSE direction.

In this thesis, I have observed ways in which deformation bands impact permeability in the Mixing Bowl study area. According to Fossen and Bale (2007), deformation bands can be found as individual structures, occurring together as clusters and in fault damage zones. They also reported that unlike fractures that generally lead to improvements in porosity and permeability in rocks, deformation bands reduce permeability in their host rocks up to six orders of magnitude, hence they tend to affect the flow of fluids. Results obtained after utilizing the t-test statistical approach on permeability data gotten from the field show that the undeformed Harding Sandstone is the most permeable with a mean permeability of 1415189 mD, and the deformation band Harding Sandstone is the least permeable. This is consistent with the work of Fossen and Bale (2007), who reported that deformation bands when present in porous sandstones tend to reduce permeability in their host rocks. The bivariate plot of permeability and distance (Fig. 43) reveals that permeability increases from the fault core to the damage zone for quarzitified Harding Sandstone but stays almost unchanged for the deformation bands sandstone.

Thin sections from deformed Harding Sandstones within the damage zones of faults reveal evidence of grain boundary migration which is indicative of a high strain and low temperature environment (Fig. 20).

# CHAPTER SIX

## Conclusion

Anlian (2017) concluded that the Cañon City Embayment (CCE) in Colorado was a megascopic syncline, composed of Ordovician to Tertiary sedimentary rocks deposited on Proterozoic basement which were all affected by several major faults of Laramide orogeny. This research and previous work did not explain the anomalous contacts between rock units like those of Fountain Formation and Harding Sandstone or Fountain and Fremont etc. In my current research, we have observed that this is not entirely true as we have provided evidence of features not only related to the Laramide orogeny, but those associated to the Ancestral Rock Mountain orogeny.

By documenting the tectonostratigraphy of the area, I was able to provide a possible explanation for the unusual stratigraphic relationship between rock units in the CCE. Rock units in the embayment are juxtaposed with each other through depositional contacts, fault contacts or unconformities. It has been confirmed that the contact between the Dakota Sandstone, Morrison Formation and Ralston Creek Formation are depositional in nature. These are the youngest and most recent deposits in the area.

The N-S thrust fault in the CCE affected rocks of the Precambrian Basement, Ordovician Harding and slightly cuts through the Pennsylvanian Fountain Formation. Because the youngest Formation it affected is the Fountain Formation, this means that the fault must have been created during or after the Pennsylvanian time which is consistent with the timing of the occurrence of the Ancestral Rocky Mountains orogeny. Hence, it is a first generation thrust fault. This Ancestral Rocky fault is crosscut by an unconformity that separates the Fountain Formation and the Basement. This unconformity is concluded to be Permian in age or younger and therefore, a first generation unconformity. A second generation of unconformity separates the Jurassic Ralston Creek and Precambrian Basement. Based on the principles of cross-cutting relationships, it must be younger than the first generation unconformity and therefore this feature must be much younger than Permian.

According to the tectonostatigraphy of the area, the E-W trending fault affected all the rocks from Proterozoic age to Jurassic. Because the youngest unit affected by this fault in the CCE is Jurassic, this fault is consistent in age with the Laramide orogeny which has been reported by previous workers to occur between late Cretaceous – Paleocene. This fault is a second generation thrust fault.

Evidence of Ancestral uplifts have been observed by the presence of the first-generation unconformity that serves as the contact between the Pennsylvanian Fountain Formation and the Ordovician Harding Sandstone. Also, the presence of quarzitified Harding Sandstone within the damage zone of the thrust fault that is found in the central region of the study area serves as evidence of the Ancestral Rocky Mountain event, although radiometric age dating is needed to verify the age of this fault.

REFERENCES


Anlian, E. Q. (2017). Deformation bands records oblique-slip faulting in the Cañon City Embayment, Colorado (Master's thesis). https://getd.libs.uga/pdfs/anlian_edward_q_201705_ms, pp. 143.

Barbeau, D. L. (2003). A flexural model for the Paradox Basin: Implications for the tectonics of the Ancestral Rocky Mountains: A flexural model for the Paradox Basin. *Basin Research*, *15*(1), 97–115. https://doi.org/10.1046/j.1365-2117.2003.00194.

Berg, S. S., & Skar, T. (2005). Controls on damage zone asymmetry of a normal fault zone: Outcrop analyses of a segment of the Moab fault, SE Utah. *Journal of Structural Geology*, *27*(10), 1803–1822. https://doi.org/10.1016/j.jsg.2005.04.012.

Bergh, S., and Snoke, A., (1992) Polyphase Laramide deformation in the Shirley Mountains, south central Wyoming foreland: *Mountain Geologist*, v. 29, no. 3, pp. 85–100.

Billi, A., Salvini, F., & Storti, F. (2003). The damage zone-fault core transition in carbonate rocks: Implications for fault growth, structure and permeability. *Journal of Structural Geology*, *25*(11), 1779–1794. https://doi.org/10.1016/S0191-8141(03)00037-3.

Bird, P. (1998). Kinematic history of the Laramide orogeny in latitudes 35°-49°N, western United States. *Tectonics*, *17*(5), 780–801. https://doi.org/10.1029/98TC02698.

Blackstone, D. L., (1990) Rocky Mountain foreland structure exemplified by the Owl Creek Mountains, Bridger Range, and Casper Arch, central Wyoming: *Wyoming Geological Association, Guidebook 41*, pp. 151–166.

Blakey, R. C., Ranney, W. D., Blakey, R. C., & Ranney, W. D. (2018). The continental arc, Sevier orogeny, Western Interior Seaway and flat-slab subduction: Cretaceous period: Ca. 145–65 Ma. *Ancient Landscapes of Western North America: A Geologic History with Paleogeographic Maps*, 103-130.

Brewer, J. A., Smithson, S. B., Oliver, J. E., Kaufman, S., & Brown, L. D. (1980). The Laramide orogeny: Evidence from COCORP deep crustal seismic profiles in the Wind River mountains, Wyoming. *Tectonophysics*, *62*(3–4), 165–189. https://doi.org/10.1016/0040-1951(80)90191-2.

Brown, D. W. (1978). Reflection seismic study of the Canon City-Pueblo area, Fremont and Pueblo counties, Colorado, A. *1970-1979-Mines Theses & Dissertations*.

Budnik, R. T. (1986). Left-lateral intraplate deformation along the ancestral rocky mountains: Implications for late Paleozoic plate motions. *Tectonophysics*, *132*(1–3), 195–214. https://doi.org/10.1016/0040-1951(86)90032-6.

Bump, A. P., & Davis, G. H. (2003). Late Cretaceous–early Tertiary Laramide deformation of the northern Colorado Plateau, Utah and Colorado. *Journal of Structural Geology*, *25*(3), 421-440.

Burbank, D. W., & Vergés, J. (1994). Reconstruction of topography and related depositional systems during active thrusting. *Journal of Geophysical Research: Solid Earth*, *99*(B10), 20281-20297.

Burchfiel, B. C., Zhiliang, C., Hodges, K. V., Yuping, L., Royden, L. H., Changrong, D., & Jiene, X. (1992). *The South Tibetan detachment system, Himalayan orogen: Extension contemporaneous with and parallel to shortening in a collisional mountain belt.* Geological Society of America. https://doi.org/10.1130/SPE269.

Caine, J. S., Evans, J. P., & Forster, C. B. (1996). Fault zone architecture and permeability structure. *Geology*, *24*(11), 1025. https://doi.org/10.1130/0091-7613(1996)024.

Carrapa, B., DeCelles, P. G., & Romero, M. (2019). Early Inception of the Laramide Orogeny in Southwestern Montana and northern Wyoming: Implications for Models of Flat-Slab Subduction. *Journal of Geophysical Research: Solid Earth*, *124*(2), 2102–2123. https://doi.org/10.1029/2018JB016888.

Chapin, C. E., and Cather, S. M., (1981) Eocene tectonics and sedimentation in the Colorado Plateau–Rocky Mountain area: *Arizona Geological Digest*, v. 14, pp. 175–198.

Chapin, C.E., Kelley, S. A., & Cather, S. M. (2014). The Rocky Mountain Front, southwestern USA. *Geosphere*, 10(5), 1043 – 1060.

Chase, R. B., Schmidt, C. J., and Genovese, R. B., (1993) Influence of Precambrian rock compositions and fabrics on the development of Rocky Mountain foreland folds; in Schmidt, C. J., Chase, R. B., and Erslev, E. A. (eds.), Laramide basement deformation in the Rocky Mountain foreland of the western United States: *Geological Society of America, Special Paper 280*, pp. 45–72.

Chester, F. M., Evans, J. P., & Biegel, R. L. (1993). Internal structure and weakening mechanisms of the San Andreas Fault. *Journal of Geophysical Research: Solid Earth*, *98*(B1), 771–786. https://doi.org/10.1029/92JB01866.

Coe, A. L. (Ed.). (2010). *Geological field techniques*. John Wiley & Sons.

Coney, P.J., 1971, Cordilleran tectonic transitions and motion of the North American plate: Nature, v. 233, p. 462-465.

Copeland, P., Currie, C. A., Lawton, T. F., & Murphy, M. A. (2017). Location, location, location: The variable lifespan of the Laramide orogeny. *Geology*, *45*(3), 223–226. https://doi.org/10.1130/G38810.1.

DeCelles, P. G., Gray, M. B., Ridgway, K. D., Cole, R. B., Pivnik, D. A., Pequera, N., & Srivastava, P. (1991). Controls on synorogenic alluvial-fan architecture, Beartooth Conglomerate (Palaeocene), Wyoming and Montana. *Sedimentology*, *38*(4), 567-590.

DeCelles, P. G., Pile, H. T., & Coogan, J. C. (1993). Kinematic history of the Meade thrust based on provenance of the Bechler conglomerate at Red Mountain, Idaho, Sevier thrust belt. *Tectonics*, *12*(6), 1436-1450.

DeCelles, P. G., Tolson, R. B., Graham, S. A., Smith, G. A., Ingersoll, R. V., White, J., Schmidt, C.J., Rice, R., Moxon, I., Lemke, L. and Handschy, J.W. (1987). Laramide thrust-generated alluvial-fan sedimentation, Sphinx Conglomerate, southwestern Montana. *AAPG Bulletin*, *71*(2), 135-155.

DeVoto, R. H., Kent, H. C., & Porter, K. W. (1980). Pennsylvanian stratigraphy and history of Colorado. *Colorado Geology: Rocky Mountain Association of Geologists*, 71-101.

Dickinson, W. R., & Lawton, T. F. (2003). Sequential intercontinental suturing as the ultimate control for Pennsylvanian Ancestral Rocky Mountains deformation. *Geology*, *31*(7), 609-612.

Dickinson, W. R., and Lawton, T. F., (2001). Carboniferous to Cretaceous assembly and fragmentation of Mexico: *Geological Society of America Bulletin*, v. 113, p. 1142–1160.

Dickinson, W. R., and Snyder, W. S., (1978) Plate tectonics of the Laramide Orogeny, in Matthews, V., ed., Laramide folding associated with basement block faulting in the western United States: *Geological Society of America Memoir 151*, p. 355–366.

English, J. M., & Johnston, S. T. (2004). The Laramide Orogeny: What Were the Driving Forces? *International Geology Review*, *46*(9), 833–838. https://doi.org/10.2747/0020-6814.46.9.833.

Erslev, E. A., and Rogers, J. L., (1993) Basement-cover geometry of Laramide fault-propagation folds; in Schmidt, C. J., Chase, R., and Erslev, E. A. (eds.), Laramide basement deformation in the Rocky Mountain foreland of the western United States: *Geological Society of America, Special Paper 280*, pp. 339–358.

Erslev, E. A., Holdaway, S. M., O'Meara, S., Jurista, B., Selvig, B., Cather, S. M., ... & Kelley, S. A. (2004). Laramide minor faulting in the Colorado Front Range. *New Mexico Bureau of Geology and Mineral Resources*, *160*, 181-203.

Erslev, E. A., Worthington, L. L., Anderson, M. L., & Miller, K. C. (2022). Laramide crustal detachment in the Rockies: Cordilleran shortening of fluid-weakened foreland crust. *Rocky Mountain Geology*, *57*(2), 65–97. https://doi.org/10.24872/rmgjournal.57.2.65.

Faulkner, D. R., Jackson, C. A. L., Lunn, R. J., Schlische, R. W., Shipton, Z. K., Wibberley, C. A. J., & Withjack, M. O. (2010). A review of recent developments concerning the structure, mechanics and fluid flow properties of fault zones. *Journal of Structural Geology*, *32*(11), 1557–1575. https://doi.org/10.1016/j.jsg.2010.06.009.

Flynn, J.L. and Barber, L.B., 2000, Quality of ground-water and surface water in an area of individual sewage disposal system usage near Barker Reservoir, Nederland, Colorado, August-September, 1998: U.S. Geological Survey, Open-File Report 00-214, 8 p.

Fossen, H., & Bale, A. (2007). Deformation bands and their influence on fluid flow. American Association of Petroleum Geologists Bulletin, 91, 1685– 1700.

Fossen, H., Soliva, R., Ballas, G., Trzaskos, B., Cavalcante, C., & Schultz, R. A. (2018). A review of deformation bands in reservoir sandstones: Geometries, mechanisms and distribution. *Geological Society, London, Special Publications*, *459*(1), 9–33. https://doi.org/10.1144/SP459.4.

Frederickson, E. A., Lay, J.M.D., & Saylor, W. W. (1956). Ralston Formation of Canon City Embayment, Colorado. American Association of Petroleum Geologists Bulletin, 9, pp. 2120-2148.

Fuis, G. S., Moore, T. E., Plafker, G., Brocher, T. M., Fisher, M. A., Mooney, W. D., Nokleberg, W.J., Page, R.A., Beaudoin, B.C., Christensen, N.I., Levander, A.R., & Ruppert, N. A. (2008). Trans-Alaska Crustal Transect and continental evolution involving subduction underplating and synchronous foreland thrusting. *Geology*, *36*(3), 267-270.

Gerhard, L.C. (1967). Paleozoic Geologic Development of Canon City Embayment, Colorado. *AAPG Bulletin, 51.* https://doi.org/10.1306/5D25C26F-16C1-11D7-8645000101C1865D.

Goldstein, A. G. (1981). Comment and Reply on 'Plate tectonics of the Ancestral Rocky Mountains' COMMENT. *Geology*, *9*(9), 387-388.

Gong, J. (1986). The evolution of the Canon City Embayment, Colorado. Oklahoma State University, (Master's thesis), pp. 146.

Gries, R. R., (1983) North-south compression of the Rocky Mountain foreland structures; in Lowell, J. D., and Gries, R. R. (eds.), Rocky Mountain foreland basins and uplifts: *Rocky Mountain Association of Geologists*, pp. 9–32.

Hansen, W. R., (1986) History of faulting in the eastern Uinta Mountains, Colorado and Utah; in Stone, D. S., and Johnson, K. S. (eds.), New interpretations of northwest Colorado Geology: *Rocky Mountain Association of Geologists*, pp. 5–17.

Haun, J. D., & Kent, H. C. (1965). Geologic history of Rocky Mountain region. *AAPG Bulletin*, *49*(11), 1781-1800.

Holmes, C. N. (1956). Tectonic history of the ancestral Uncompahgre Range in Colorado: Internt. Assoc. Pet. Geol. Guidebook – Seventh Annual Field Conference, pp. 29 – 37.

Hoy, R. G. and Ridgway, K. D. (2002). Syndepositional thrust-related deformation and sedimentation in an Ancestral Rocky Mountains basin, central colorado trough, colorado, usa. Geological Society of America Bulletin, 114(7), 804-828.

Hoy, R. G., & Ridgway, K. D. (1997). Structural and sedimentological development of footwall growth synclines along an intraforeland uplift, east-central Bighorn Mountains, Wyoming. *Geological Society of America Bulletin*, *109*(8), 915-935.

Kluth, C. F. and Coney, P. J. (1981). Plate tectonics of the Ancestral Rocky Mountains. *Geology*, 9(1), 10.

Kluth, C. F., and Nelson, S. N., (1988) Age of the Dawson Arkose, Southwestern Air Force Academy, Colorado, and implcations for the uplift history of the Front Range: *The Mountain Geologist*, vol. 25, no. 1, pp. 29–35.S.

Kluth, C. F., Ye, H., Royden, L., Burchfiel, C., & Schuepbach, M. (1998). Late Paleozoic deformation of Interior North America: The Greater Ancestral Rocky Mountains: Discussion & Reply. *AAPG bulletin*, *82*(12), 2272-2276.

Laubach, S.E., Eichhubl, P., Lander, R.H., 2010. Structural diagenesis. J. Struct. Geol. 32, 1866–1872. https://doi.org/10.1016/j.jsg.2010.10.001.

Lawton, T. F. (1985). Style and timing of frontal structures, thrust belt, central Utah. *AAPG Bulletin*, *69*(7), 1145-1159.

Lawton, T. F., & McMillan, N. J. (1999). Arc abandonment as a cause for passive continental rifting: Comparison of the Jurassic Mexican Borderland rift and the Cenozoic Rio Grande rift. *Geology*, *27*(9), 779-782.

Leary, R. J., Umhoefer, P., Smith, M. E., & Riggs, N. (2017). A three-sided orogen: A new tectonic model for Ancestral Rocky Mountain uplift and basin development. *Geology*, G39041.1. https://doi.org/10.1130/G39041.1.

Lindsey, D. A., Andriessen, P. A. M., & Wardlaw, B. R. (1986). Heating, cooling, and uplift during Tertiary time, northern Sangre de Cristo Range, Colorado. *Geological Society of America Bulletin*, *97*(9), 1133-1143.

Lindsey, D. A., Johnson, B. R., & Andriessen, P. A. M. (1983). Laramide and Neogene Structure of the Northen Sangre De Cristo Range, South-Central Colorado.

Liu, S., & Currie, C. A. (2016). Farallon plate dynamics prior to the Laramide orogeny: Numerical models of flat subduction. *Tectonophysics*, *666*, 33–47. https://doi.org/10.1016/j.tecto.2015.10.010.

Lowell, J. D., (1983) Foreland deformation; in Lowell, J. D, and Gries, R. R.. (eds.), Rocky Mountain foreland basins and uplifts: *Rocky Mountain Association of Geologists*, pp. 1–8.

Maxson, J., & Tikoff, B. (1996). Hit-and-run collision model for the Laramide orogeny, western United States. *Geology*, *24*(11), 968. https://doi.org/10.1130/0091-7613(1996)024<0968:HARCMF>2.3.CO;2.

Monger, J. W. H., and Nokleberg, W. H., (1996). Evolution of the northern North American Cordillera: Generation, fragmentation, displacement, and accretion of successive North American plate margin arcs, in Geology and ore deposits of the American Cordillera: Reno, NV, *Geological Society of Nevada*, p. 1133–1152.

Monger, J. W. H., Price, R. A., and Tempelman-Kluit, D. J., (1982) Tectonic accretion and the origin of the two major metamorphic and plutonic welts in the Canadian Cordillera: *Geology*, v. 10, p. 70–75.

Moucha, R., Forte, A.M., Rowley, D.B., Mitrovica, J.X., Simmons, N.A., and Grand, S.P., (2008). Mantle convection and the recent evolution of the Colorado Plateau and the Rio Grande.

New England Research. Inc., 2014. User's Manual for the TinyPerm II. White River Junction, VT.

Oldow, J. S., Bally, A. W., Ave Lallemant, H. G., and Leeman, W. P., (1989) Phanerozoic evolution of the North American CordilleraUnited States and Canada; in Bally, A. W., and Palmer, A. R. (eds.), The geology of North America, an overview: *Geological Society of America*, v. 1A, pp. 139–232.

Passchier, C. W., & J., Trouw, R. A.J. (2005). *Microtectonics* (2nd ed). Springer.

Rift valley: Geology, v. 36, n. 6, p. 439-442.

Rodrigues, R. de S., Alves da Silva, F. C., & Cordoba, V. C. (2021). Evolution of deformation bands, insights from structural diagénesis. *Journal of Structural Geology*, 143. http://doi.org/10.1016/j.jsg.2020.104257.

Soreghan, G. S., Keller, G. R., Gilbert, M. C., Chase, C. G., & Sweet, D. E. (2012). Load-induced subsidence of the Ancestral Rocky Mountains recorded by preservation of Permian landscapes. *Geosphere*, *8*(3), 654-668.

Stone, D. S., (1986) Seismic and borehole evidence for important preLaramide faulting along the axial arch in northwest Colorado; in Stone, D. S, and Johnson, K. S. (eds.), New interpretations of northwest Colorado Geology: *Rocky Mountain Association of Geologists*, pp.19–36.

Sweet, D. E., & Soreghan, G. S. (2010). Application of quartz sand microtextural analysis to infer cold-climate weathering for the equatorial Fountain Formation (Pennsylvanian–Permian, Colorado, USA). *Journal of Sedimentary Research*, *80*(7), 666-677.

Sweet, D. E., Brotherton, J. L., Chowdhury, N. U. M. K., & Ramsey, C. E. (2021). Tectonic subsidence analysis of the Ancestral Rocky Mountains from the interior to the southern margin. *Palaeogeography, Palaeoclimatology, Palaeoecology*, *576*, 110508. https://doi.org/10.1016/j.palaeo.2021.110508.

Thomas, P. C., Veverka, J., Belton, M. J., Hidy, A., A'Hearn, M. F., Farnham, T. L., Groussin, O., Li, J.Y., McFadden, L.A., Sunshine, J. & Delamere, W. A. (2007). The shape, topography, and geology of Tempel 1 from Deep Impact observations. *Icarus*, *187*(1), 4-15.

Torabi, A., & Berg, S. S. (2011). Scaling of fault attributes: A review. *Marine and Petroleum Geology*, *28*(8), 1444–1460. https://doi.org/10.1016/j.marpetgeo.2011.04.003.

Torabi, A., Ellingsen, T. S. S., Johannessen, M. U., Alaei, B., Rotevatn, A., & Chiarella, D. (2020). Fault zone architecture and its scaling laws: Where does the damage zone start and stop? *Geological Society, London, Special Publications*, *496*(1), 99–124. https://doi.org/10.1144/SP496-2018-151.

Tweto, O. (1980). Precambrian geology of Colorado. *Colorado geology: Rocky Mountain Association of Geologists*, 37-46.

Tweto, O., (1975) Laramide (Late Cretaceous–early Tertiary) orogeny in the Southern Rocky Mountains; in Curtis, B. F. (ed.), Cenozoic history of the Southern Rocky Mountains: *Geological Society of America, Memoir 144*, pp. 1–44.

Warner, L. A. (1983). Comment and Reply on ‘Plate tectonics of the Ancestral Rocky Mountains’ COMMENT. *Geology*, *11*(2), 120-121.

Webster, G. D. (1959). Geology of the Canon City – Twin Mountain area, Fremont County, Colorado. (Master’s thesis, University of Kansas), pp. 99.

Weimer, R. J., Kent, H. C., & Porter, K. W. (1980). Recurrent movement on basement faults, a tectonic style for Colorado and adjacent areas. *Colorado geology: Rocky Mountain Association of Geologists*, 23-35.

Ye, H., Royden, L., Burchfiel, C., & Schuepbach, M. (1996). Late Paleozoic Deformation of Interior North America: The Greater Ancestral Rocky Mountains. *AAPG Bulletin*, *80*. https://doi.org/10.1306/64ED9A4C-1724-11D7-8645000102C1865D.